Investigations on Nitrogen Doped Graphene Synthesized by Modified Chemical Vapor Deposition

A Dissertation submitted to the
Graduate School of Science and Engineering
in partial satisfaction of the requirements for
the degree of

Master of Science

in

Materials Science and Engineering

By

Navid Solati Eskandar

KOÇ
UNIVERSITY

January 23, 2017

Koç University

Graduate School of Sciences and Engineering

This is to certify that I have examined this copy of a master's thesis by

Navid Solati Eskandar

and have found that it is complete and satisfactory in all respects,
and that any and all revisions required by the final
examining committee have been made.

Committee Members:

Asst. Prof. Dr. Sarp Kaya

Assoc. Prof. Dr. Uğur Ünal

Assoc. Prof. Dr. Adem Tekin

Date: 23.01.2017

ABSTRACT

Graphene, fundamental building block of carbon based materials, has gained more attention from both scientific and technological communities not only due to its unique properties such as quantum hall effect at room temperature, tunable band gap, high elasticity, and an ambipolar electric field effect but also due to its electrochemical functionalities. Within a plane of graphene, which consists of honeycomb lattice of sp^2 hybridized carbon atoms, there are three in plane σ bonds and one π orbital for each of the atoms. This bonding nature difference provide spectacular properties anisotropy for graphene. Starting from the early years of last decade that science community's focus was brought to bear on graphene, various synthesis techniques have been developed. Among those, mechanical exfoliation and epitaxial growth have gained more attention. However, low crystallinity of the former one and lack of scalability of the latter, are the main drawbacks of these methods. Chemical Vapor Deposition (CVD) of various carbon precursors on different substrates opened a new era in reaching to a desired low cost, high quality and large scale graphene.

Beside feasibility of pristine graphene to be used in different applications, it is possible to modify its properties with different chemical methods and to introduce new features to it. One of the main strategies in graphene modification is chemical doping. Addition of a foreign element into its bonding network can turn graphene into electrochemically active material. Nitrogen doped graphene is a new type of metal free electro-catalyst which offers great potential in terms of activity, durability and selectivity. Several methods have been proposed to synthesize N doped graphene. These methods, which generally are classified to direct synthesis and post treatment, include different types of nitrogen precursors such as NH_3, N_2, N_2H_4, etc. as well as various synthesis techniques like CVD, segregation, plasma treatment, etc. The main features which determine the electrochemical activity of N doped graphene are nitrogen concentration and its configuration in graphene lattice. It is well-known that nitrogen has three possible configuration (pyridinic, pyrrolic and graphitic) in graphene with different electrochemical properties.

In this study, multi-layer graphene films in centimeter scale were synthesized by CVD method on multi-crystalline Cu foils. Methane was used as the precursor of carbon. The impacts of different parameters such as total pressure, growth time, growth temperature, methane flow rate and heating rate were investigated in a great detail by the application of Raman spectroscopy. Graphene has some obvious fingerprints in its Raman spectrum that make it possible to determine both the quality of the graphene film (from defect density point of view) and also the number of layers. The results showed that copper substrate temperature and hydrogen exposure time are two important control parameters in order to have a high crystalline graphene. Moreover, the total pressure of the system was found to be critical. The presence of hydrogen at elevated temperatures (900 °C and higher) makes the Cu surface smooth, eliminate the contaminations and enlarge grain size.

CVD grown graphene was doped with nitrogen atoms by using N_2 plasma. The results obtained from Raman spectroscopy and microscopy, X-ray photoelectron spectroscopy (XPS) and also atomic force microscopy (AFM) were cross-examined to investigate homogeneity of nitrogen doping distribution as well as its atomic configuration. It was proved that more than 35% nitrogen was doped into the graphene structure including all three types of C-N bonding.

Further investigations indicated that pyridinic and pyrrolic sites are the most favorable configurations and nitrogen atoms tend to occupy these sites at low nitrogen coverage. Heat treatment of these samples did not result in a configurational change. However, in N doped graphene samples with high concentration of nitrogen, where all three types of nitrogen were present, heating up to mild temperatures caused graphitic nitrogen to get converted to pyridinic and pyrrolic nitrogen, which are presumably more electrochemically active. The sp^2 honeycomb structure of graphene was not damaged during heat treatment.

ÖZET

Karbon temelli materyallerin temel yapı taşı olan grafen, oda sıcaklığında kuantum hall etkisi, ayarlanabilir bant aralığı, yüksek elastikiyet ve elektrokimyasal işlevsellikleri gibi eşsiz özelliklerinden ötürü son yıllarda hem bilimsel hem de teknolojik topluluklardan yüksek ilgi görmüştür. sp^2 hibridize karbon atomlarının petek kafeslerinden oluşan grafenin bir düzleminde, her atom için üç düzlemsel σ bağları ve bir π orbital vardır. Bu bağlanma doğası farkı, grafen için olağanüstü anizotropi özelliklere sağlar. Geçen on yılın başlarından itibaren Bilim topluluğunun grafen odaklanmasına dayanarak çeşitli sentez teknikleri bu madde için geliştirildi. Bunların arasında mekanik eksfoliyasyon ve epitaksiyel büyüme daha fazla ilgi görmüştür. Ancak, düşük kristallik ve ölçeklenirlik eksikliği, bu yöntemlerin temel dezavantajlarıdır. Çeşitli karbon prekürsörlerinin farklı alt katmanlar üzerinde kimyasal buhar birikimi (CVD), arzulanan düşük maliyetli, yüksek kaliteli ve büyük ölçekli grafen ulaşmada yeni bir çağ açtı.

Değişik uygulamalarda bozulmamış grafenin fizibilitesinin yanı sıra özelliklerini değişik kimyasal yöntemlerle değiştirmek ve yeni özellikler eklemek mümkündür. Grafen değiştirmedeki ana stratejilerden biri kimyasal katkılamada bulunmaktır. Bağlanma ağına yabancı bir element eklenmesi, grafeni elektrokimyasal olarak aktif materyale dönüştürebilir. Azotla katkılı grafen (N katkılı grafen), aktivite, dayanıklılık ve selektivite bakımından büyük bir potansiyel sunan metalden bağımsız yeni bir elektrokatalizör türüdür. N katkılı grafenin sentezlenmesi için çeşitli yöntemler önerilmiştir. Genellikle doğrudan sentez ve sentez den sonar işleme tabi tutulmak üzere sınıflandırılan bu yöntemler, NH_3, N_2 ve N_2H_4 gibi farklı türde azot öncüllerinin yanı sıra CVD, ayırım ve plazma işlemi gibi çeşitli sentez teknikleri içerir. N katkılı grafenin elektrokimyasal aktivitesini belirleyen başlıca özellikler, azot konsantrasyonu ve grafen kafesindeki konfigürasyonudur. Azotun, grafen kafesinde üç olası konfigürasyonuna (piridinik, pirolik ve grafitik) sahip olduğu iyi bilinmektedir.

Bu çalışmada, santimetre ölçekli çok katmanlı grafen filmleri CVD tekniği ile çok kristalli Cu folyolar üzerine sentezlenmiştir. Karbonun öncüsü olarak metan kullanıldı. Toplam basınç, büyüme süresi, büyüme sıcaklığı, metan akış hızı ve ısıtma hızı gibi farklı parametrelerin etkileri Raman spektroskopisinin uygulanmasıyla ayrıntılı bir şekilde incelendi. Grafen, Raman spektrumunda, filmin kalitesini (kusur yoğunluğu açısından bakıldığında) hem de katman sayısını belirlemeyi mümkün kılan bazı belirgin parmak izlerine sahiptir. Sonuçlar, yüksek kristalin bir grafen sahip olmak için bakır yüzey sıcaklığı ve hidrojen maruziyet süresinin iki önemli kontrol parametresi olduğunu göstermiştir. Üstelik sistemin toplam basıncı kritik olarak bulundu. Yüksek sıcaklıklarda (900 °C ve üzeri) hidrojen varlığı, Cu yüzeyini pürüzsüz hale getirir, kirleticileri ortadan kaldırır ve tane boyutunu büyütür.

CVD yontemiyle büyümüş grafen, N_2 plazması kullanılarak azot atomları ile katkilanmiştir. Raman spektroskopisi ve mikroskopi, X-ışını fotoelektron spektroskopisi (XPS) ve ayrıca atomik kuvvet mikroskopisi (AFM) ile elde edilen sonuçlar, atomik konfigürasyonun yanı sıra azot katkılama dağılımının homojenliğini araştırmak için çapraz incelendi. Her üç C-N bağını içeren % 35'den fazla azotun grafen yapısına katkılanmış olduğu kanıtlandı. Daha ileri araştırmalar, piridinik ve pirrolik alanların en uygun konfigürasyonlar olduğunu ve nitrojen atomlarının bu yerleri düşük azot kapsamında işgal etme eğiliminde olduğunu belirtti. Bu numunelerin ısıl işlemi, her hangi bir yapılandırma değişikliğine sebep olmadı. Ancak, üç azot tipinin de mevcut olduğu yüksek azot konsantrasyonuna sahip grafen numunelerinde, hafif sıcaklıklara kadar ısınma, grafitik azotun piridinik ve pirolik azota dönüştürülmesine neden oldu. Isıl işlem sırasında grafenin sp^2 petek yapısında hasar görülmedi.

ACKNOWLEDGEMENTS

I would like to thank my advisor Asst. Prof. Dr. Sarp Kaya, who has guided me throughout my research with his patience and knowledge. He was always keen about my project and never let me feel that he is tired of my endless questions. It was a great pleasure to have long discussions with a talented and highly motivated person like him.

I want to express my sincere thanks to my thesis committee members Assoc. Prof. Dr. Adem Tekin and Assoc. Prof. Dr. Uğur Ünal.

My sincere thanks go to the Scientific and Technological Council of Turkey (TUBITAK) (Project number: 113Z654), Graduate School of Sciences and Engineering and Koç University TÜPRAŞ Energy Center (KUTEM) for providing support and giving me the opportunity to work on this project.

Special thanks to Dr. Rıza Kızılel for supporting me during last two years in KUTEM and also to Dr. Barış Yağcı, Cansu Yıldırım and Dr. Amir Motallebzadeh for patiently teaching me how to use Raman spectroscopy, SEM, FTIR and AFM instruments, for performing numerous measurements.

Although it was very difficult to be far from my home, but it was pure luck for me to meet with awesome friends in KUTEM, the only part of the university where there is always people working. Special thanks to all KUTEM members who made my master studies sheer bliss.

I owe more than thanks to my beloved soul-mate Mahshid Hashemkhani. Thank you for providing me moral support throughout this experience and for being always by my side.

Finally, my very special gratitude goes to my family, who provided me unconditional support during my whole life and take great delight with any success that I have. You showed me true love can be felt even when there is thousands of kilometers distance.

To my parents Neda and Reza and my brother Milad

Table of Contents

List of Figures:

Chapter 1
Introduction

1.1. Graphene

Graphene is a two-dimensional sheet of sp^2-hybridized carbon. It is known as parent of all graphitic forms because its extended honeycomb network is the basic building block of other important allotropes; it can be stacked to form 3D graphite, rolled to form 1D nanotubes (CNT), and wrapped to form 0D fullerenes [1]. Graphene exhibits unique properties which have fascinated the scientific community and has made it one of the major research topics in the last decade. Historically, the studies of graphite to utilize fewer and fewer layers delivered a jolt in 2004, when Geim and co-workers at Manchester University first isolated single-layer samples from graphite using micro-mechanical cleavage method [2].

Ideally graphene is a single-layer material, but graphene samples with two or more layers are being investigated with equal interest. Three different types of graphenes can be defined: single-layer graphene (SG), bilayer graphene (BG), and few-layer graphene (FG) [3]. Bi-layer and few-layer graphenes have 2 and 3 to 10 layers of two-dimensional carbon sheets, respectively. Thick graphene sheets which consist of more than 10 layers are of less scientific interest [4]. There are different ways for C atoms to be stacked in bi- and few-layer graphene, generating hexagonal or AA stacking, Bernal or AB stacking and rhombohedral or ABC stacking. Within a plane each carbon shows three in-plane σ bonds and one π orbital perpendicular to the plane. While the strong σ bonds work as the rigid backbone of the hexagonal structure, the out-of plane π bonds control interaction between different graphene layers [5].

The most important properties of graphene are a quantum Hall effect at room temperature [6], tunable band gap, high elasticity [3], and an ambipolar electric field effect along with ballistic conduction of charge carriers [2]. The anisotropy of graphene properties fascinate both scientists and technologists. The origin of this property is the obvious difference between in plane and out of plane bonds nature, which leads to an out of plane electrical and thermal conductivities 103 times lower than those of their in-plane analogues [1].

1.2. Nitrogen Doped Graphene

There are various morphologies of graphene with different behavior and properties. For example the increased concentration of a zigzag edge tends to decrease band gap of graphene [7]. As a consequence, modification on the morphology of graphene has become one of the main strategies to alter its properties. Chemical doping is another important approach to tailor the properties of graphene, which can be divided to two main classifications: (a) the adsorption of gas, metal or organic molecules to the graphene surface [8]–[10] and (b) substitutional doping, where replacement of carbon atoms with heteroatoms, such as nitrogen and boron, is the main approach.

Theoretical and experimental studies have shown that nitrogen doping can tune the chemically derived functionalized graphene from being a p-type to n-type semiconductor [11]. Shao et al. have also investigated electrochemical properties of N doped graphene. According to their results, not only the electrocatalytic activity of N doped graphene in reduction of oxygen and H_2O_2 is much higher than pristine graphene, but also it exhibits much higher durability and selectivity than the widely-used and expensive Pt. They suggested that the enhanced performance is mainly attributed to nitrogen functional groups in N doped graphene [12].

Similar to the synthesis of N-CNT, N doped graphene can be obtained through two different ways: direct synthesis and post treatment. Despite theoretical studies which suggested that direct synthesis may lead to create a homogeneous doping throughout the bulk material, the results reported so far fail to indicate so. Specifically, direct synthesis includes chemical vapor deposition (CVD), segregation growth, solvothermal, and arc-discharge approaches. Post treatment includes thermal treatment, plasma treatment, and N_2H_4 treatment.

In a typical nitrogen doped graphene CVD approach, a mixture of gases containing carbon and nitrogen atoms are introduced to flow over a metallic catalyst substrate at high temperature. These precursors dissociate and recombine into N doped graphene by means of precipitation on the surface of the catalyst [13]–[15]. Apart from the gas mixture, liquid organic precursors have also been used to form N doped graphene [16]. Nitrogen-containing boron layers and carbon-containing nickel layers are sequentially deposited on the SiO_2/Si substrate by electron beam evaporation, in order to synthesis nitrogen doped graphene by segregation growth. The final step in this method is vacuum annealing process, during which the boron atoms are trapped by nickel, and the carbon atoms will segregate out onto the nickel surface and combine to form N doped graphene [17]. In the last direct N doped graphene synthesis method, which is known as solvothermal approach, lithium nitride (Li_3N) is mixed with tetrachloromethane (CCl_4) at 250^o C in autoclave. The product of this reaction is graphene sheets with 1-6 layers which has an average of about 5% nitrogen content [18].

One of the post treatment approaches is thermal treatment which refers to the method using high temperature to produce N doped graphene. Different groups have shown that heating graphene in NH_3 at high temperature ($\geq$800 °C) can produce N doped graphene. The nitrogen content in the N doped graphene synthesized by this method is relatively low. For example, the highest nitrogen content that Guo et al. obtained was 1.1% doping level at 1100

°C [19]; this content for the samples prepared by Geng et al. was 2.8% at 900 °C [20]. The low doping level may be attributed to two reasons: one is the insufficient defect number in the high quality graphene, and the other is the high annealing temperature, which will break the C−N bonds in N doped graphene. Reducing graphene oxide in a mixture of NH_3 and N_2H_4, which is known as hydrazine hydrate (N_2H_4) treatment, is another strategy to prepare N doped graphene. The nitrogen content reaches up to 5 % at reduction temperature of 80 °C; however, a significant portion of nitrogen content is as absorbed N_2H_4. In order to desorb N_2H_4, the reaction temperature should be 160 °C or higher. Long et al. have shown that the nitrogen content decreases to ~4 % at this temperature [21].

When carbon material is placed in the nitrogen plasma atmosphere, carbon atoms will be partly replaced by nitrogen atoms; therefore, N doped graphene could be prepared from graphene by exposing it to the nitrogen plasma [22], [23]. NH_3 plasma has also been used to obtain N doped graphene [24]. One of the main advantageous of this method is that the nitrogen content, which varies from 3 to 8.5 % in different works [25], can be controlled by the plasma strength and exposure time. The creation of defects and oxygen-containing groups are side effects of plasma exposure process. The graphene samples prepared by Shao et al. contained 3.5 % oxygen species; this number jumped to 8.6 % after doping nitrogen in graphene by plasma [12]. Almost the same ratio between oxygen contents before and after exposing graphene to the plasma has reported by Wang et al. [26]. The reactive carbon atoms at the edge of defects that are created by the plasma treatment are the main oxygen containing sites [12].

Nitrogen atoms can have three different configurations in the graphene lattice, including quaternary N (or graphitic N), pyridinic N, and pyrrolic N (Figure 1). Specifically, N atoms that substitute for C atoms in the hexagonal ring are known as graphitic N, while pyridinic refers to a configuration in which nitrogen atom bonds with two C atoms, contributing one p

electron to the π system. These two types are sp^2 hybridized ones. In addition there is a third group (Pyrrolic N) which has sp^3 hybridization. Pyrrolic N bonds into the five-membered ring and contributes two p electrons to the π system [25]. Apart from these three common nitrogen types, nitrogen oxides of pyridinic N have been observed [12].

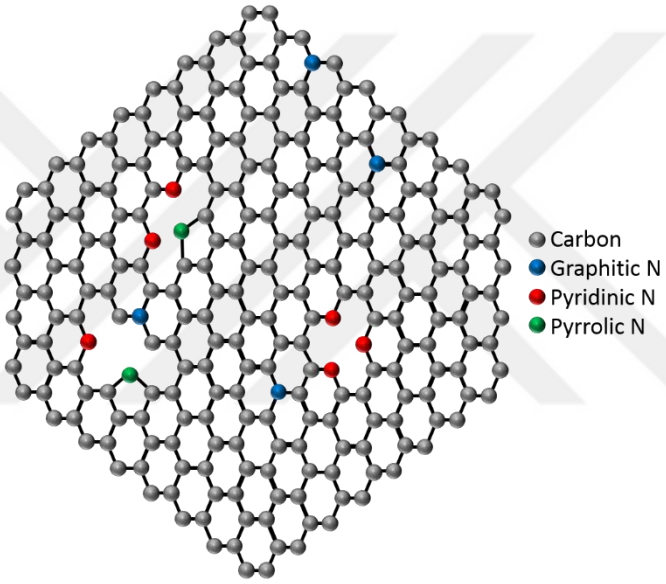

Figure 1 Different bonding configurations of nitrogen atoms in graphene lattice

1.3. Electrochemical Applications of N doped Graphene

N doped graphene is a potential candidate for technological applications such as lithium ion batteries, ultracapacitors and fuel cells. A fuel cell is an electrochemical energy conversion device that oxidizes fuel (H_2, CH_4, etc.) at the anode and reduces oxygen from air at the cathode to produce electricity [27]. High conversion efficiency, high power density and clean operation (no pollution) make fuel cells attractive. Commonly, Pt and its alloys, [28] are used as the catalyst for the oxidation reaction on the anode and reduction reaction

on cathode. However, the large scale applications of Pt catalysts are limited by its high cost, scarcity, time-dependent drift, and CO poisoning [29]. Thus, there have been intensive research efforts, to reduce or replace Pt and Pt based alloys electrodes in fuel cells [30]–[32].

Oxygen reduction reaction on cathode is the key point that affects the chemical-electrical energy conversion in fuel cell. This reaction dominates the overall performance of a fuel cell because it is a kinetically slow process, [33]. Theoretically there are two pathways for ORR. One is a direct four-electron pathway, in which O_2 is reduced directly to water without involvement of hydrogen peroxide,

$$O_2 + 4H^+ + 4e^- \rightarrow 2H_2O$$

The second one, which is less efficient, is two-step two-electron pathway in which hydrogen peroxide is formed as an intermediate,

$$O_2 + 2H^+ + 2e^- \rightarrow H_2O_2$$

To achieve a fuel cell with high efficiency, the four-electron pathway is desired reaction. In order to overcome the kinetic obstacles of ORR process, catalysts must be used to facilitate the four electron pathway to boost the efficiency of fuel cells. Recently, N doped graphene has been used in fuel cells as either the catalysts directly or carbon support to anchor metal catalysts. The N doped graphene synthesized in this study will be used as cathode part of the fuel cells in future researches.

Zhang et al. revealed that the major factors determining the catalytic active sites of N doped graphene in ORR are spin density and charge density of atoms. As a result of unpaired electron which are introduced by the substitution of N atoms in graphene structure, the atomic charge distribution will change. The active sites in N doped graphene usually are carbon atoms that possess high spin density [34].

Several investigations have recently performed on metal-free N doped graphene with enhanced catalytic activity toward ORR [12], [35], [36] The efficiency of ORR can be evaluated through two ways [37]. One way is to calculate the transferred number of electrons through the Koutecky−Levich equations by using a rotating disk electrode (RDE);

$$\frac{1}{j} = \frac{1}{j_L} + \frac{1}{j_K} = \frac{1}{(B\omega^{\frac{1}{2}})} + \frac{1}{j_K} \quad \text{Equation 1}$$

$$B = 0.62nFC_0(D_0)^{3/2}\nu^{-1/6} \quad \text{Equation 2}$$

$$j_K = nFkC_0 \quad \text{Equation 3}$$

Where j is the measured current density, j_K and j_L are the kinetic- and diffusion-limiting current densities, ω is the angular velocity of the rotating disk, n is the overall number of electrons transferred in ORR, F is the Faraday constant, C_0 is the bulk concentration of O_2, D_0 is diffusion coefficient of O_2, ν is the kinematic viscosity of the electrolyte, and k is the electron transfer rate constant, respectively [38]. Another way is to measure the proportion of H_2O_2 formed during the ORR process by using a rotating ring disk electrode. Using the first method Qu et al. [39] showed that while the two-electron pathway is the running process in pristine graphene ORR, N doped graphene exhibited a typical one-step, four-electron ORR pathway, which is similar to the ORR pathway of a Pt catalyst. In another approach, which investigated the catalytic efficiency of N doped graphene through the second method, the H_2O_2 formed in the ORR process was about 10% at −0.5 V in the diffusion-controlled region. This result indicated the four electron reduction process dominates in ORR [20]. All these studies show that N doped graphene can be a very effective catalyst for ORR.

Furthermore, there are some researches which compare the stability of N doped graphene with commercial Pt bases catalyst. Shao et al. investigated the electrocatalytic activity of Pt based and N doped graphene cathodes before and after Accelerated Degradation Test (ADT).

They reported that the Pt based cathode has higher electrocatalytic activity than N doped graphene before the test, but after the ADT, due to the degradation of Pt cathode, the N doped graphene exhibits higher kinetic current [12]. These advantages make N doped graphene a promising candidate for ORR in fuel cells.

The N doped graphene catalysts in most of the above studies, where the four-electron ORR pathway was observed, consist of two or three nitrogen types. Different groups have tried to investigate the effect of each individual nitrogen types on efficiency of these catalysts. Lue et al. [36] suggested that for N doped graphene possessing only the pyridinic N, a two-electron reduction process is the major ORR pathway. As a result, pyridinic N may not be the desired type of nitrogen atoms in graphene structure for fuel cell applications. However, on account of the scarcity of study in this field and effect of different experimental conditions on the results, the relationship between the catalytic activity and the nitrogen species is still debatable. The first step in making these effects clear is to design a synthesis method in which the type of the nitrogen can be under control.

In addition to nitrogen types, the nitrogen content can also affect the ORR activity of N doped graphene. However, there are lots of studies with contradictory results in this field. Because N doped graphene usually consists of two or three nitrogen types and the content of different nitrogen types usually varies with different nitrogen doping levels [18], [35] and as mentioned above, different nitrogen types have various electrochemical effects. As a result, the only studies that can be directed here are the ones with only one type of nitrogen. In one of these studies where N doped graphene contains only pyridinic N, the sample with higher nitrogen content (16%) had poorer ORR activity in comparison with the one which had lower nitrogen content (2.2%) [36]. Theoretical studies have been shown that number of oxygen molecules adsorbed on the surface of graphene during ORR as well as the strength of their bonds with graphene sheets increase with increase in number of N atoms doped in the

structure of graphene [40]. This confirms the results obtained by Luo et al. and suggests that an optimal nitrogen content might be critical to achieving a high ORR activity.

Apart from investigation on N doped graphene as catalyst, several studies also have studied the efficiency of Pt/N doped graphene in both oxidation and reduction reactions [22], [41] [42]. The nitrogen atoms do not bond with Pt directly; instead, they direct a Pt atom to bond with the carbon atom, which is more energetically favored. The substitution of N atoms in graphene disrupts the double bond in graphene structure which doubles the binding energy between Pt and carbon atoms. This is helpful to prevent Pt nanoclusters from migrating and forming larger particles. As a result, the catalytic durability of Pt will be improved [25]. Existence of nitrogen in the structure of graphene helps Pt to disperse better on the surface of N doped graphene [41]. Moreover, the conductivity of N doped graphene improves at high temperatures (~800 °C). The last mentioned two factors make Pt/N doped graphene exhibit a 3 times higher oxidation current than Pt/carbon black catalyst. The stronger bonds between C and Pt in Pt/N doped graphene compared with Pt/graphene catalyst beside better dispersion of Pt atoms, improves Pt/N doped graphene performance when it used for oxygen reduction reaction [22], [42].

Despite vast number of published papers about synthesis and characterization of N doped graphene as a potential material for electrochemical applications, there is still a lack of evidence and lots of unsolved questions about them. In this project we tried to found a correlation between different characterization methods to quantify properties of N doped graphene. In addition, considering the importance of type of doped nitrogen in graphene and the fact that due to the nature of CVD method usually it is not possible to apply same synthesis parameters in different CVD machines and prepared the same graphene, the feasibility of post synthesis methods (such as heating) to modify type of nitrogen has investigated. Finally, the main step in converting graphene from a potential materials for

energy storage application to a commercial one is to increase operation time and efficiency of graphene based electrodes. We aimed to increase percentage of homogenously doped nitrogen graphene in order to increase amount of active area on it during electrochemical reactions.

Chapter 2
Experimental

2.1. Chemical Vapor Deposition (CVD)
2.1.1. The CVD System

To coat an object (the ‘‘substrate’’) with a thin film, it is often preferred to put it in an atmosphere of atoms and/or molecules of the precursor. These vapor-based thin film synthesis methods are classified as either physical vapor deposition (PVD) or chemical vapor deposition, depending on whether the film deposition process is driven by physical impacts or by chemical reactions, which occur between precursors, precursor’s fragments and the substrate, respectively. The atmosphere is often consist of diluted precursor molecules in a carrier gas that makes up the main part of the gas volume in the process. In the case of growing large area and high quality graphene on metal substrates CVD is a very promising technique [43].

The CVD system used in this project is composed of three basic stages:

2.1.1.1. Gas Delivering System

The growth gases necessary for CVD of graphene are methane and hydrogen. There are mass flow controllers that deliver required amount of these gases precisely. The flow rate of each gas is regulated by unit called ‘standard cubic centimeter per minute’ (sccm). The presence of the relatively large amounts of argon gas, in comparison to the hydrogen and methane, helps displace any oxygen or water vapor present in the chamber, allowing for a cleaner growth process. These three gases are mixed properly before being fed into the reacting system (quartz tube). The gases fed in get involved in chemical reactions which

result in synthesizing graphene films on substrates at high temperature and low pressure of the system [44].

2.1.1.2. Reacting System

Due to high growth temperatures, usually a quartz tube is used as the growth chamber. Melting point of the quartz tube is as high as 1670 °C (β tridymite) and 1717 °C (β cristobalite) which makes it a suitable material of choice for sustaining at high temperatures. The quartz tube is mounted onto the CVD furnace and care is ensured that it is exactly at a center point of the furnace. This is to ensure that temperature is evenly distributed on both sides of the tube. A temperature of ~1100 ^{o}C can be reached in ~84 minutes with this furnace.

2.1.1.3. Gas Removal System

The removal system involves a vacuum pump connected to the same end of the quartz tube where the gas inlet flow controllers are connected (as can be seen in Figure 2). This pump sucks out the necessary amount of air or gas from the tube to keep it under the stated pressure level. The required pressure depends on substrate and also characteristics of required graphene such as number of layers, uniformity, etc. The system is capable of reaching a base pressure of ~2 mTorr.

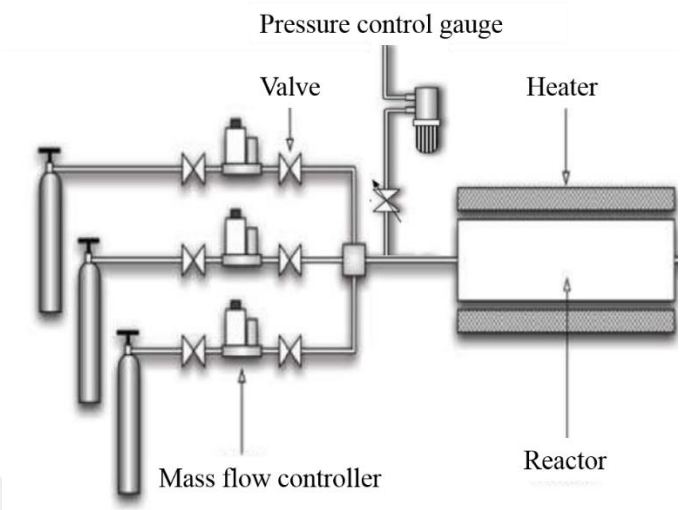

Figure 2 Schematic of the CVD system

2.1.2. Theory of Chemical Vapor Deposition

Thin film growth by CVD is the result of a complex sequence of surface and/or gas phase chemical reactions (pyrolysis, reduction, oxidation, co-deposition, etc.). These reactions are schematically summarized in Figure 3. As a result of the fluid dynamics when flowing a gas mixture above the surface, a boundary layer develops on top of the substrate surface. This layer has a major role in CVD because, both the velocity and concentration of species are significantly different than that in the main gas stream. The lower speed of the species in the boundary layer makes almost all chemistry of importance to the CVD process to take place in this layer and on the substrate surface.

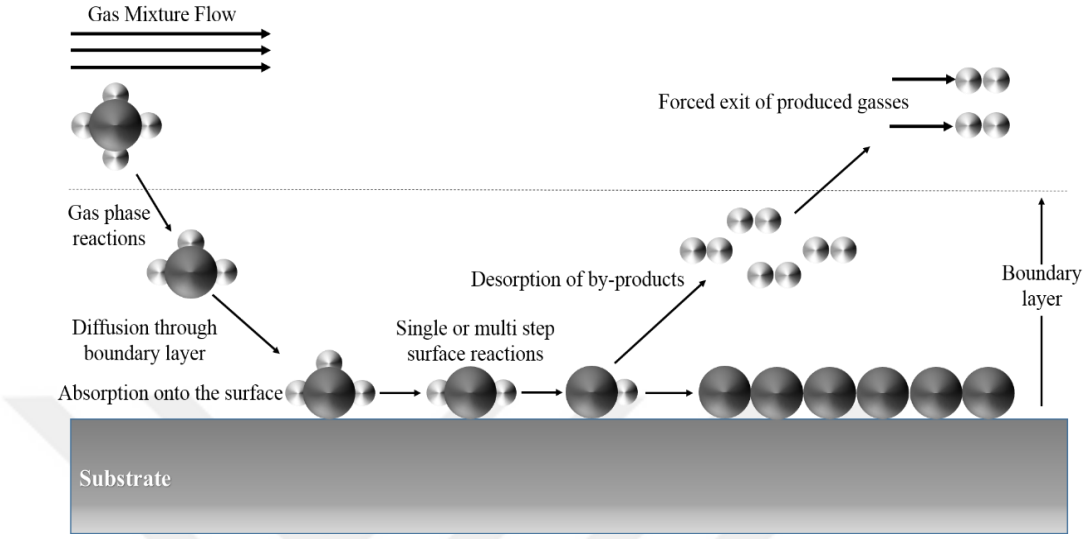

Figure 3 Most important chemical reactions involved in chemical vapor deposition technique

CVD processes are usually done at low pressures and high temperatures, allowing a significant lifetime of very reactive species, compared to many other chemical reaction environments. These reactive species are formed due to the gas phase chemical reactions. These gas phase reactions become more important at higher temperatures and low total reactor pressures. Many CVD systems are operated in ways that minimize gas-phase reactions in order to avoid particle formation that could interfere with the desired film deposition. In contrast, other CVD systems utilize gas-phase reactions to convert reactant molecules that are relatively unreactive at the surface into more reactive species.

The precursor molecules or the more reactive fragments of the precursor molecules are transported via gas diffusion through the boundary layer to the substrate surface. All types of precursor molecules can be expected to weakly physisorb at least for a short time, on the substrate followed by desorption. Sufficient chemical complementarity between precursor or reactive fragment and substrate surface results in stronger chemisorption, leading to longer lifetimes of the adsorbate. Adsorbate molecules or fragments may be mobile on the surface and may sample a variety of surface sites via diffusion, which again may lead to reactions.

At the final step, the parts of the precursor molecule that do not constitute the target material desorb from the film surface as by-products.

From kinetics point of view, the whole CVD process can be classified to two main category, the mass transport part and surface reactions. As a result, the slowest of these categories determines if the process is mass transport or surface reaction limited. At lower temperatures the deposition rate is generally surface reaction limited. As the temperature increases, the surface reaction rate rises exponentially, resulting in a mass transport limited deposition [45].

2.1.3. Factors Impacting CVD Growth of Graphene

The most important factors that impact the graphene growth in the chemical vapor deposition technique are as follows:

- Total and partial pressures of the gases
- Hydrocarbon source
- Temperature
- Hydrogen
- Substrate
- Pre-treatment of copper

Each of these factors has different impact on every substrate. Following a brief discussion about the effect of each of these factors is reported:

2.1.3.1. Pressure

Although, there are some reports about high pressure large area graphene growth by chemical vapor deposition (HPCVD), Low pressure (LPCVD) has been mainly preferred for single or bilayer graphene [46]. Most of the groups have chosen 0.5 Torr as the border pressure to classify the synthesis method to above mentioned two groups. Any change in the pressure will affect the kinetics of the process but the thermodynamics are the same at any pressure level. High pressure usually releases the source gas at a higher turbulence whereas

low pressure tends to provide a smooth flow of the source gas with lower turbulence. This results in better interaction between the gases and the substrate which in contrast with the high pressure scenario where the turbulence would result in collisions. As a result, there will be an instantaneous deposition or lesser efficient interactions between the substrate and the gases. Therefore high pressure growths usually result in a lower quality graphene when compared to a low pressure growth [47]. However, depending on the concentration of the other gases used in the growth process and other ambient conditions, the amount of optimum pressure varies in different CVD systems. In addition to the total pressure of the system, partial pressure of each of the gases is an important factor in determining the quality of graphene. Higher partial pressure of a gas means higher concentration of it available on the surface of the substrate, which affects the properties of the graphene due to the unique impacts of different gaseous species during CVD process.

2.1.3.2. Hydrocarbon Source

Thermodynamics of a CVD growth of graphene on copper using various hydrocarbon sources show similarities. The catalytic dissociation of saturated and unsaturated hydrocarbon molecules occur at a certain cracking temperature and then the carbon atoms on the substrate bind to each other to form graphene. Different hydrocarbon sources have different cracking temperatures. The lower the cracking temperature, the better it is for low temperature growths. Hydrocarbons like benzene have yielded graphene at temperatures as low as 300 °C [48]. However, due to the health concerns over benzene, the safest yet productive hydrocarbon gases which are mainly used for CVD growth of graphene are methane and ethylene.

a) Methane**:**

Methane is a hydrocarbon gas with the chemical formula CH_4, which contains only single bonds. It is known as the simplest alkane, the main component of natural gas, and probably the most abundant organic compound on earth. Methane usually requires a high temperature of ~900 °C for graphene growth.

b) Ethylene**:**

Ethylene is an organic, colorless and flammable gas, a hydrocarbon with the formula C_2H_4. This compound which is the simplest alkene has a much lower cracking temperature in comparison with methane. It can be used to perform growths at temperatures as low as 550 °C and hence it is very suitable for low temperature growths [49].

2.1.3.3. Temperature

The synthesis temperature is dependent on both the substrate and the hydrocarbon being used. Generally, the formation of graphene on transition metals through CVD follows a two-step mechanism. The first step is the dilution or decomposition of carbon precursor on the metal catalyst, which is then followed by the formation of a graphene. Temperature is the main source of energy for the decomposition of carbon precursors and for the activation of a catalyst. For a typical CVD, the temperature in the range of 800–1000 °C is usually employed for most of the catalysts, such as Cu, Ni, Ru and Pt, to grow graphene sheets [50]. When copper is used as the substrate, due to its filled 3d shell which results in a very low activity and carbon solubility [51], high temperature is required for graphene to form. It has been reported that graphene can be formed at a temperature of below 850 ºC through CVD using Cu catalyst but the graphene sheet will contain large amount of defects [52]. Generally, lower temperature causes the formation of high density and small area graphene; whereas, high temperature forms low density and large area graphene. This is ascribed by higher adsorption of hydrocarbon onto the Cu surface that causes denser nucleation at a relatively low temperature [53].

2.1.3.4. Hydrogen

The presence of hydrogen is a must in the growth of graphene using CVD technique. Hydrogen acts differently with different substrates. It readily diffuses in Cu, while it recombines on the Ni surface. The main reason for these different actions relies on different hydrogen diffusion coefficients with Cu and Ni. In general hydrogen has three major purposes:

a) Graphene formation:

It plays a major role in "dehydrogenation" of hydrocarbon gases, which defines as the breaking down process of the hydrocarbon molecules into hydrogen and carbon [54], [55]. There exists a competition between the "dissociative chemisorption" nature of H_2 and the "dissociative dehydrogenation" of CH_4 on the surface sites. This H_2 competition plays a kinetic inhibitor role mainly for graphene growth on Cu.

Dehydrogenation of hydrocarbons (in this case methane) is represented by the following equations:

$$CH_4(s) + (s) \rightarrow CH_3(s) + H(s)$$
$$CH_3(s) + (s) \rightarrow CH_2(s) + H(s)$$
$$CH_2(s) + (s) \rightarrow CH(s) + H(s)$$
$$CH(s) \rightarrow C(s) + H(s)$$

Where (s) represents surface sites.

This process is hindered by the surface hydrogen. Consequently, the increase of hydrogen could drastically reduce the amount of graphene formation on the surface of Cu [56].

Above mentioned effect of hydrogen is highly dependent on the substrate, for example in the Ni case, the hydrogen that tends to comes out to the surface helps the dehydrogenation of the hydrocarbons, whereas in the case of Cu, the same hydrogen combines with surface hydrogen and stays on the surface itself, this obstruct the dehydrogenation of hydrocarbons. Therefore a carefully balanced amount of hydrogen is to be used for growths on Cu [57].

b) Layer Control:

Hydrogen removes excess layers of carbon from the substrate by hybridization of sp^2 carbon to sp^3 [54], [55]. These hybridized carbon atoms then leave the surface as a hydrocarbon (mostly CH_4) at a particularly low pressure, high temperature and considerable amount of H_2 flow. Therefore, in addition to act as an inhibitor for dehydrogenation of

methane during graphene growth, it also participates in controlling the number of layers of graphene and layer size by etching it. On Cu, the etching occurs noticeably at temperatures no less than 850 °C.

c) Oxide Layer Removal Prior to Growth:

The H_2 treatment before graphene growth is done because of the need to remove native oxides layers on substrates. Hydrogen combines easily with oxygen atoms on the surfaces and hence it removes the native oxide layer away from the metal which in this case is copper.

2.1.3.5. Substrate

From copper and nickel to iron, cobalt, platinum, iridium and ruthenium, a wide range of transition metal substrates can be used in graphene CVD growth. Among these substrates copper and nickel are the ones that have attracted attention of different research groups, due to their unique properties [44].

a) Copper:

The most important property of copper which makes it suitable substrate for synthesis of graphene is its almost zero carbon solubility. Therefore, the dehydrogenated hydrocarbon gas can interact with the Cu substrate and deposits carbon onto the surface of Cu in the presence of a carrier gas and hydrogen at low pressure and high temperature. Islands of graphene are the first structures that formed on the surface of Cu which in turn result into flakes upon further deposition. Combination of these flakes and formation of a layer of graphene are the next steps of graphene growth [58]. After the first layer graphene is deposited, Cu surface is fully covered and there is no catalyst exposed to hydrocarbon to promote decomposition and growth. As a result, the graphene grown on Cu substrate is expected to be monolayer, however existence of some steps on the surface of copper provides a chance for new flakes to grow in further accumulation. In a controlled CVD process done on pretreated copper substrate, the percentage of these new layers won't be higher than ~5 [59].

b) Nickel:

Although, Nickel has non-negligible carbon solubility and as result, there is a stronger graphene-metal interaction, but its lattice parameters match better with graphene compared to copper and also there are no tilt grain boundaries in nickel as there is in copper. Graphene formation in nickel happens during cooling where the solubility of nickel reduces and therefore the excess dissolved carbon precipitates to the surface. The carbon atoms which precipitate out of the nickel, pick the high energy areas such as grain boundaries and they do not arrange themselves in a uniform manner. The result is absence of uniformity in graphene synthesized on nickel. Therefore, cooling is the most important step in synthesis of graphene on nickel. Rapid cooling results in less graphene because there is not enough time for carbon precipitation to occur, meanwhile there won't be any graphene on nickel in a process with slow cooling, because carbon atoms diffuse deep into the bulk catalyst.

2.1.3.6. Copper Annealing

The process of copper annealing happens when copper is brought close to its melting point of 1084.2 ^{o}C. There are two main goals to operate this process before graphene growth. Un-annealed copper foil generally has lines across its surface that are due to their production process. In order to eliminate these lines and have large flat plateaus, copper atoms need to get specific amount of energy to rearrange themselves. This energy would be supplied, when the temperature of copper is brought near its melting point. Also new surface morphology created by annealing contains large flat plateaus, that are more conducive for the growth of a two dimensional material like graphene [60]. The importance of having large grains relies on the fact that the boundaries are likely locations for the formation of graphene nucleation sites. So a large flat plateau would reduce the number of nucleation sites. Fewer nucleation sites would allow for larger graphene domains to grow and reduce the chance of secondary graphene growth. The other effect of heating copper to such high temperatures results in the elimination of most residual contaminations on the surface of the copper. These two effects suggest that graphene quality should improve with higher annealing times.

2.1.4. Chemical Vapor Deposition of Graphene

The graphene film synthesis was performed in a NANOVAK Plasma Enhanced Chemical Vapor Deposition (PECVD) system. A 25μm thick copper foil (Sigma-Aldrich, 99.8% purity) was used as the substrate. The general scheme of synthesis process was started by cutting a 5x5 cm^2 piece of copper foil and placing it into the PECVD chamber by support of a quartz sample holder. The system then was evacuated and heated up to a certain temperature under Ar atmosphere and then hydrogen was inserted to the system in order to make the copper surface smooth and clean (we call this step "hydrogen treatment"). By reaching to the synthesis temperature methane was introduced to the gas combination and synthesis was started. Finally, the system was cooled down to room temperature under hydrogen and argon atmosphere.

The effects of different parameters such as heating rate of copper substrate, time and temperature of hydrogen treatment step, time and temperature of synthesis and also flow rate of each three used gases (argon, hydrogen and methane) during different steps as well as total pressure of the system have investigated. In order to do so, the synthesis strategy divided to two main groups, based on total pressure of the system. First group was synthesized at ~ 0.5 Torr and was named as "Low pressure" (LPCVD) samples. The pressure for the second group ("high pressure" (HPCVD) samples) was chosen among 4, 5 and 6 Torr. A set of synthesis parameters were chosen as initial parameters and the first low pressure sample was synthesized by heating up the substrate with a rate of 5 ^oC/min to 900 ^oC under 100 sccm of Ar flow. Hydrogen treatment step was lasted for 90 minutes by adding 50 sccm of H_2 to the system followed by graphene growth step which proceeded at 900 ^oC for 45 minutes. The gas mixture contained 100, 20 and 10 sccm of argon, hydrogen and methane; respectively. Finally, the sample was cooled down to room temperature under 100 sccm of Ar.

The first modification was done on the flow rate of methane, where in addition to the initial sample, 3 sets of samples with 5, 20 and 30 sccm of methane were synthesized. Further investigations on effect of parameters were carried out by preparing samples with different

synthesis time (45, 30 and 15 minutes) and different synthesis temperatures (850 and 900 ^{o}C) for low pressure samples. Then, the synthesis process was done at different total pressures (0.5, 4, 5 and 6 Torr) to determine impact of this parameter. Finally the flow rate of methane and also heating rate were modified in HPCVD samples. The synthesized samples were then transferred to silicon substrates which were coated with 300 nm thick SiO_2.

2.2. Plasma

2.2.1. Plasma Generation and Theory

A plasma is an ionized gas consisting of positively and negatively charged particles with approximately equal charge densities. The charged particles are generated by supplying energy to a neutral gas [61]. Plasmas can be produced by heating an ordinary gas to such a high temperature that the random kinetic energy of the molecules exceeds the ionization energy. Collisions then strip some of the electrons from the atoms, forming a mixture of electrons and ions. Because the ionization process starts at a fairly well-defined temperature, usually a few thousand K, a plasma is often referred to as the "fourth" state of matter. Plasmas can also be produced by exposing an ordinary gas to energetic photons, such as ultraviolet light or X-rays [62]. Adiabatic compression of the gas is also capable of heating up a gas to the point of plasma generation. Yet another way to supply energy to a gas reservoir is via energetic beams that moderate in a gas volume. Beams of neutral particles have the added advantage of being unperturbed by electric and magnetic fields [63].

The most commonly used method of generating and sustaining a low-temperature plasma for technological and technical application is by applying an electric field to a neutral gas. Any volume of a neutral gas always contains a few electrons and ions that are formed, for example, as the result of the interaction of cosmic rays or radioactive radiation with the gas. These free charge carriers are accelerated by the electric field and new charged particles may be created when these charge carriers collide with atoms and molecules in the gas or with the

surfaces of the electrodes. This leads to an avalanche of charged particles that is eventually balanced by charge carrier losses, so that a steady-state plasma develops.

The steady-state ionization density depends on a balance between ionization and recombination. In order to maintain a high degree of ionization, either the ionization source must be very strong, or the plasma must be very tenuous so that the recombination rate is low. The definition of a plasma requires that any deviation from charge neutrality must be very small. In the absence of a loss mechanism, the overall charge neutrality assumption is usually satisfied because all ionization processes produce equal amounts of positive and negative charge. However, deviations from local charge neutrality can occur. Usually these deviations are small, since as soon as a charge imbalance develops, large electric fields are produced that act to restore charge neutrality. Systems that display large deviations from charge neutrality, such as vacuum tubes and various electronic devices, are not plasmas, even though some aspects of their physics are similar.

To create a plasma the charged particles must be in an unbound gaseous state. This requirement can be made more specific by requiring that the random kinetic energy be much greater than the average electrostatic energy, and is imposed to provide a distinction between a plasma, in which the particles move relatively freely, and condensed matter, such as metals, where electrostatic forces play a dominant role. In a plasma, long-range electrical forces are much more important than short-range forces. Long-range forces lead to many complex effects that do not occur in an ordinary gas. Plasmas can be divided into two broad categories: natural and man-made. It is an interesting fact that most of the material in the visible universe, as much as 99% according to some estimates, is in the plasma state. This includes the Sun, most stars, and a significant fraction of the interstellar medium [62].

There are characteristic parameters that are the most fundamental parameters relevant to the description of essentially all plasma phenomena. They are:

- Number density
- Temperature

- Debye length
- Plasma frequency
- Cyclotron frequency
- Collision frequency
- Number of electrons per Debye cube

Detailed explanation and discussion about each of these parameters are out of scope of this thesis and can be found in different reference books.

A complete mathematical model of a plasma requires three basic elements: first, the motion of all particles must be determined for some assumed electric and magnetic field configuration; second, the current and charge densities must be computed from the particle trajectories; and third, the electric and magnetic fields must be self-consistently determined from the currents and charges, taking into account both internal and external sources. To be self-consistent, the electric and magnetic fields obtained from the last step must correspond to the fields used in the first step. It is this self-consistency requirement that makes the analysis of a plasma difficult.

2.2.2. Nitrogen Plasma

Nitrogen plasmas have numerous industrial applications. They are used in metal nitriding to improve surface hardness, wear and corrosion resistance and fatigue life. Nitrogen-containing plasmas are also used to treat the surfaces of organic polymers in order to change the wettability and promote adhesion [64]. Furthermore, there are many applications of nitrogen plasmas in thin film deposition [65]. Industrial plasmas operate either at low pressures (less than 1 Torr) or at atmospheric pressure.

The identification of the constituent particles and estimation of the gas temperature are the most important factors in characterization of any plasma environment. Since the dissociation of molecular nitrogen requires large energy, at least 10 eV, the first positive

system ($N_2(B^3\Pi_g\text{-}A^3\Sigma u^*)$ and the second positive system ($N_2(C^3\Pi_u\text{-}B^3\Sigma_g)$ are the most dominant constituent particles of nitrogen plasma [66]. However a non-negligible fraction of the high energy electrons, atomic nitrogen and also N^+ ions exist in the environment of nitrogen plasma as well. In the case of plasma temperature it can be evaluated from the rotational temperature of the molecules. The rotational temperature is estimated from the profile shape of the uv-visible emission spectra [66].

2.2.3. Synthesis of Nitrogen Doped Graphene

Nitrogen atoms were doped in the structure of graphene samples, prepared on both copper and SiO_2/Si substrates, using PECVD system. The samples were loaded on the same sample holder which had used for graphene growth and then the system was evacuated to a base pressure of ~2 mTorr. The plasma was ignited using 1.7 sccm of N_2 gas with a plasma power of 10 W at room temperature. After 5 minutes of exposing samples to nitrogen plasma, the system was switched off and the flow rate of nitrogen was increased to 50 sccm. The samples were kept under this atmosphere for 30 minutes to make sure that the surface of them has stabilized.

2.3. Transfer of Graphene

In order to increase processability of graphene films to be used in wafer scale devices, they should be transferred to arbitrary and desired substrates. Transfer of graphene onto some substrates such as SiO_2/Si helps to improve the characterization of it. The main goal of designing transfer methods for graphene films is to prevent structural damages to the graphene layers. However, due to the wet chemical nature of most transfer methods introduced so far, the most suitable transfer method is the one which lowers the amount of these damages and defects.

One of the main steps of transfer is to etch the metal substrate (copper, in this project). In order to do so, a polymer support (poly(methyl methacrylate) (PMMA) 4%), was attached to

the samples. This step was carried out by spin coating of PMMA onto Cu/graphene films for 30 seconds with 4000 rpm. The samples were then kept at room temperature for 3-4 hours to dry the polymer. 0.1 M Ammonium persulfate was chosen to treat the Cu/graphene/PMMA sandwiches with it and to etch the copper substrate. It is well known that ammonium persulfate is one of the solutions that introduce less defects to graphene in comparison with other etching candidates such as $FeCl_3$, HCl, H_2SO_4, etc [67]. After floating the films on ammonium persulfate over night, they were cleaned by deionized (DI) water for 15-20 min. In order to make sure about complete elimination of etching residuals, the films were again floated in DI water for 20 min. Silicon wafer with 300 nm thick oxide layer on top (SiO_2/Si) was used as the secondary substrate of graphene. It was cleaned by modified RCA (Radio Cooperation of America) method and then graphene/PMMA film was transferred on it [68]. The transferred films were kept at room temperature with 45° angle overnight to evacuate possible water molecules between graphene and SiO_2/Si. Finally, PMMA was cleaned from top of graphene by soaking the films in acetone.

2.4. Optical Microscopy (OM)

2.4.1. Theory and Instrumentation

Most of the commercially available optical microscopes consist of two main parts known as objective lens and eyepiece lens. In the simplest model of OMs these two lenses are located at the ends of the microscope body tube, which is painted matt black inside to minimize internal reflections that would contribute to glare. The theory behind the operation of optical microscope and generation of image in it, is based on both geometric optics and wave theory light. Unfortunately it is out of the scope of this thesis to explain these fields in detail, however comprehensive information about each of them can easily be found in text books [69]. Figure 4 shows the configuration of objected lens (depicted by OO) and eyepiece lens (shown with EE) in the main tube of a typical OM. Nowadays, the modern microscopes have a fixed body tube length, known as mechanical tube length, because the lenses are designed in a way that work best at a fixed mechanical tube length. This ray diagram is obtained by

considering that rays passing through the optical center of a lens move straight, but those parallel to the optic axis of the lens should pass through conjugate focal of the lens. AB in Figure 4 is the object which magnifies by the two lenses and the observer sees it as A"B".

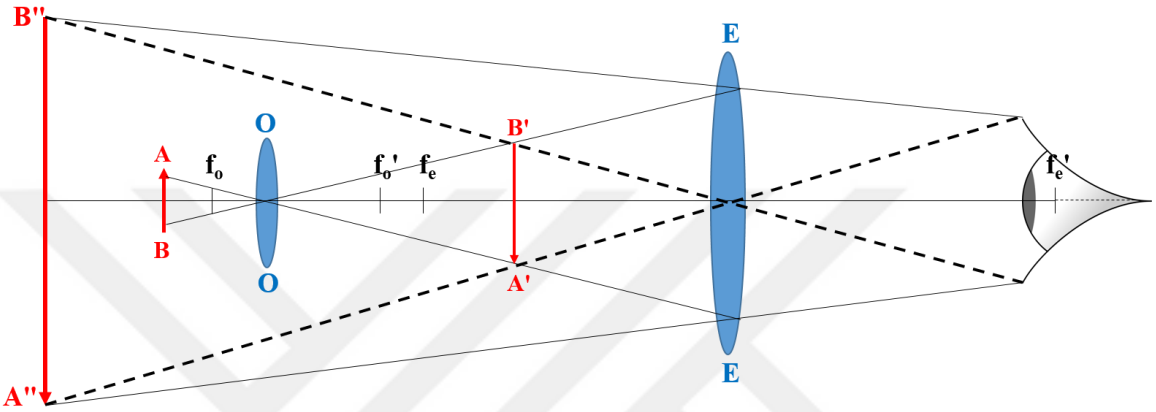

Figure 4 Ray diagram for image formation in simple optical microscope

The magnification of the system is determined by following equation:

$$M = \frac{t}{f_o}$$ Equation 4

Where t is the length of the tube and f_o stands for focal point of the objective lens.

In addition to the lenses, an illuminating system needs to be mounted to the microscope, because most of the samples are not luminous. The position of this illuminating system depends whether the microscope is going to run in transmitted or reflected mode. Figure 5 demonstrates schematic representation of a typical Optical Microscope.

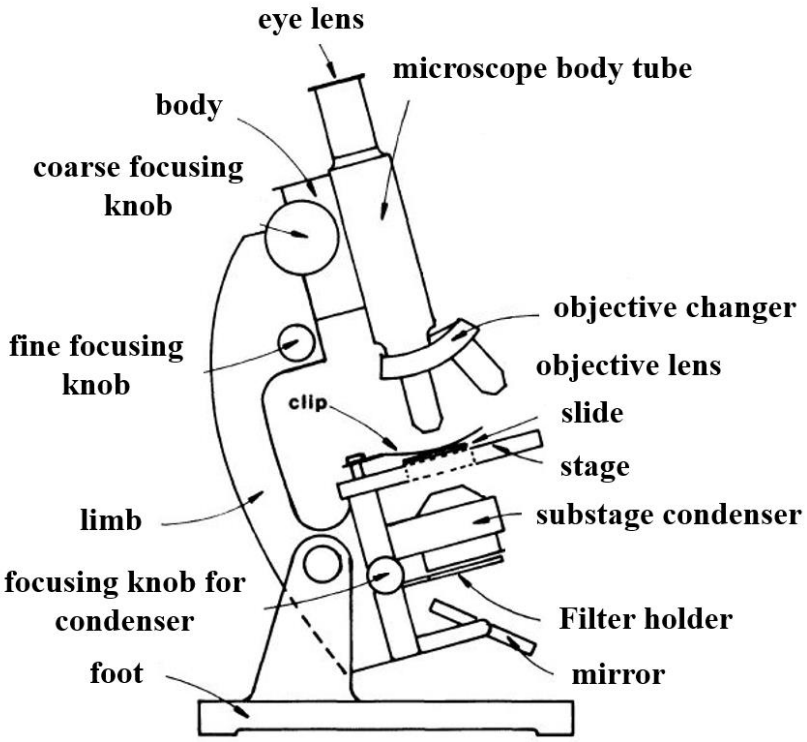

Figure 5 Schematic representation of optical microscope instrumentation. Adopted from [69].

2.4.2. OM Characterization of Graphene

The optical microscope characterization of graphene samples was done using MM500T MTI microscope. Due to the transparent nature of single and few layer graphene, it is difficult to detect it while it is on copper substrate. The problem leads most of the groups to use OM for graphene only when it is transferred onto SiO_2/Si substrate. However, Zhang et al. [70] showed that, the oxidation resistance of copper in air increases up to 325 ^oC when is covered with graphene. Consequently, it is possible to manipulate easily obtained oxidized copper surface to characterize graphene by OM on it. In this situation the parts of copper covered with graphene remain unchanged while the other parts oxidize and look reddish. This color contrast is helpful in determining whether graphene film is integrated or not. They also revealed that since higher number of layers of graphene makes it harder to oxidize underlying

copper, it is even possible to compare thickness of different parts of graphene in a precise investigation where heat treatment temperature is under full control.

2.5. Raman Spectroscopy

2.5.1. Theory

Raman spectroscopy, which is based on identifying wavelength distributions of the scattering photons from material exposed to monochromatic photons, is an efficient technique to reveal the presence of various carbon allotropes. The majority of the photons are elastically scattered which is known as Rayleigh scattering. In this case, only the direction of light is changed with no change in photon energy. Some of the photons, however, are scattered inelastically through a process known as Raman scattering. This technique can classified as vibration spectroscopy methods in which a comprehensive knowledge about vibration theory of molecules is essential. The vibrational spectrum of a molecule is composed of bands representing active normal vibrations which depends on the masses of the atoms in the molecule, the strength of their chemical bonds and the atomic arrangement. Consequently, each vibrational spectrum can be considered as a fingerprints of a specific molecule. In order to explain the Raman spectrum of a sample, it is essential to consider effect of electromagnetic field on matter. The dipole moment, P, induced in a molecule by an external electric field, E, is proportional to the field

$$P = \alpha E \qquad \text{Equation 5}$$

The proportionality constant α is the polarizability of the molecule. Raman scattering occurs because a molecular vibration can change the polarizability. The change is described by the polarizability derivative, dα/dQ, where Q is the normal coordinate of the vibration. As a result, the selection rule for a Raman-active vibration can be shown as

$$\frac{d\alpha}{dQ} \neq 0 \qquad \text{Equation 6}$$

Also Raman scattering intensity is proportional to the square of the polarizability derivative. If a vibration does not greatly change the polarizability, then the polarizability derivative will be near zero, and the intensity of the Raman band will be low.

Raman scattering occurs due to a transfer of energy to certain Raman active vibrational modes in the material. The change in energy and therefore increase or decrease in wavelength of the light is the Raman shift. The initial state of a molecule at room temperature is mostly, but not completely, the ground state and the scattered photon will have lower energy (longer wavelength) than the incident photon. This phenomena causes a Raman shift which is known as Stokes shift (or Stokes scattering).

Meanwhile a small fraction of the molecules are in vibrationally excited states. Raman scattering from these molecules leaves the molecule in the ground state and the scattered photon appears at higher energy. This process is anti-Stokes-shift and due to the lower population of excited states, it is always weaker than the Stokes-shifted spectrum, but at room temperature it is strong enough to be useful for vibrational frequencies less than about 1500 cm^{-1}.

The order of the Raman process is given by the number of scattering events that are involved in the Raman process. The most usual case is the first-order Stokes Raman scattering process, where the photon energy excitation creates one phonon in the crystal with a very small momentum ($Q \approx 0$). If two, three or more scattering events occur in the Raman process, then the process is called second-, third-, or higher-order, respectively. An interesting point in the higher-order Raman signal in a solid material is that the restriction for $Q \approx 0$ in a first-order Raman scattering process is relaxed.

2.5.2. Raman Spectrum of Graphene

Observation of the intensity, shape and position of the peaks in Raman spectrum of graphene (D, G and 2D bands) is very useful to understand its quality and to estimate the number of layers in a graphene film. The photo-excited electrons in sp^2 carbon structures are located in *k* space near the hexagonal corners of the 2D Brillouin zone, known as the K and K' points. Here, there are two possibilities for $Q \neq 0$ scattering: intra-valley (K → K, K' → K') and inter-valley scattering (K → K', K' → K). In Raman spectra of graphene and other carbon materials with dominating sp^2 hybridization of atomic bonds, most intense features are the G peak (~1587 cm^{-1}), the D peak (~1350 cm^{-1}) and the 2D peak (~2700 cm^{-1}). These peaks are always observable in graphite samples [71] (Figure 6).

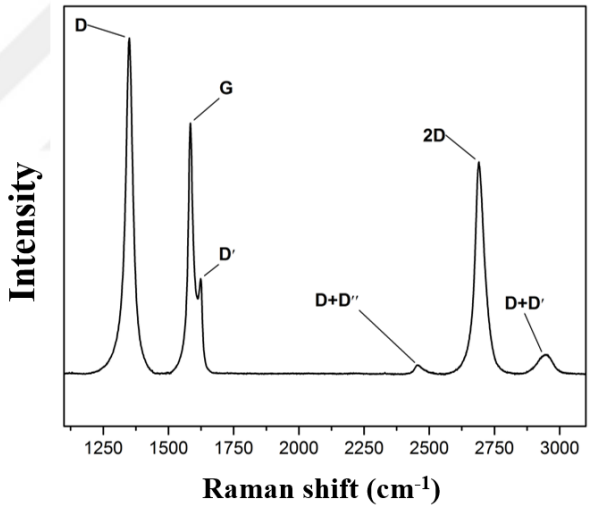

Figure 6 Typical Raman spectrum of graphene showing all main characteristic peaks of it

2.5.2.1. G Band

The G peak is located at ~1587 cm^{-1} in the graphene spectrum (Figure 6). It occurs due to the double degenerate zone center E2g mode and corresponds to the in-plane vibrational mode involving sp^2 hybridized carbon atoms [72]. This means that there are three neighbors

for every carbon atoms. The G band is produced with a first-order Raman scattering process, where the electron-hole pair generated by incident photon (shown with green arrows in Figure 7) is scattered with a phonon without any change in momentum, Q = 0 [73]. This process is pictured in Figure 7 by downward blue arrow. The G band has the ability to vary with the number of layers of graphene that are present. As the number of graphene layers increase, the planar carbon bonds become weaker and the peak shifts to lower energies. What is useful about the G peak is that its intensity and width remains relatively constant, in comparison the other characteristic peaks.

2.5.2.2. D and D' Bands

In a defective graphene where the periodic lattice of sp^2 carbon atoms is broken, the momentum conservation requirement is broken and as a result, all the phonons in the Brillouin zone become Raman active [74]. However some resonant processes like the ones showed with blue arrows connecting red bullets in Figure 7 are predominant [75]. As a result of this mechanism, the Raman spectrum of disordered graphene exhibits two new peaks at ~1350 cm^{-1} (the D band) and at ~1620 cm^{-1} (the D' band). Also a combination scattering peak (D+ D') at ~2940 cm^{-1} appears [76]. These bands, which can be seen in Figure 6, are known as the fingerprints of intervalley (D) and intravalley (D') defect-induced double-resonance scattering processes. In another point of view, these peaks can be explained as a result of a vibrational mode in sp^3 bonded carbon. The presence of sp^3 bonds suggest that the graphene is folded such a way that some of the carbon atoms are now bonded to four neighbors instead of the typical three in graphene.

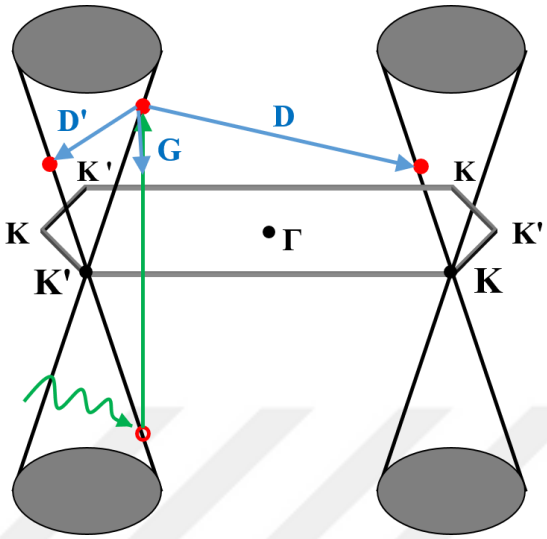

Figure 7 Schematic representation of the electronic dispersion near the fermi level at the K, K' points in the hexagonal Brillouin zone of graphene. The electron-hole pair generated by incident light (green arrow) and possible electron-phonon scattering processes resulting G, D and D' band are shown.

The absence of features related to penetration depth, makes graphene an ideal system to study defects using light as a probe. So the intensity of D and D' peaks are widely used as a sign of number of defects present. Lucchese et al. [77] have studied the evolution of disorder related peaks by taking consecutive Raman spectra of single layer graphene bombarded with Ar^+ ions. They plotted the intensity ratio of D peak to G peak (I_D/I_G) versus the average distance between the defects (L_D). As it can be seen in Figure 8, the I_D/I_G ratio was increased by decreasing the L_D, however at $L_D \sim 3.5$ nm it started to decrease. The behavior shows that there are two effective mechanisms on D peak of graphene Raman spectrum, which can be explained by the model described below.

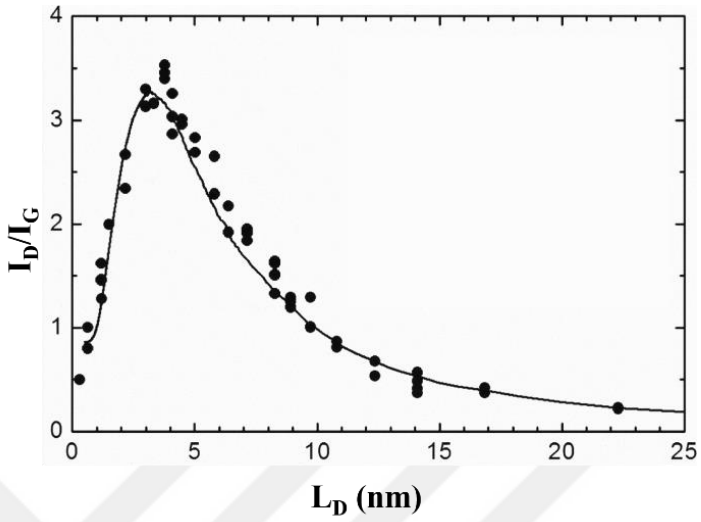

Figure 8 The I_D/I_G versus L_D plot. The defects were introduced into the graphene by Ar^+ bombardment of it. The data points are obtained three different single-layer graphene sample with various defect densities. The solid line is a modelling of the experimental data based on activated area model.

The effect of a single ion striking the single-layer graphene has two length scales. One of them is a circular area starting from impact point where structural disorder is happened (shown by red area in Figure 9a with radius of r_S) and the other one is another circular area where no disorder is introduced into the structure but selection rule has broken down due to the proximity to the structurally disordered area. The second area which is presented by blue color in Figure 9a and the radius of r_A is known as "activated area" (A region). The intensity of D peak in the activated area is locally higher than other parts of the sample. Both activated region and structurally disordered area (S region) contribute in generation of D band. However, S region has less impact because of the break-down of the graphene lattice structure in this part. In order to study the extension of A and S regions with introducing new defects, the process was simulated by randomly choosing of impact positions (Figure 9b and Figure 9c). The activated area increases by increase in number of defects (Figure 9d), which mean the intensity of D band will increase as L_D decreases. However, when the graphene sheet is almost covered with A region, more ion bombardment causes the structurally disordered region to become the dominant area of the graphene (Figure 9e), which results in

a decrease in D band intensity. Consequently, the I_D/I_G will have a non-monotonic behavior as a function of L_D, which is in agreement with Figure 8.

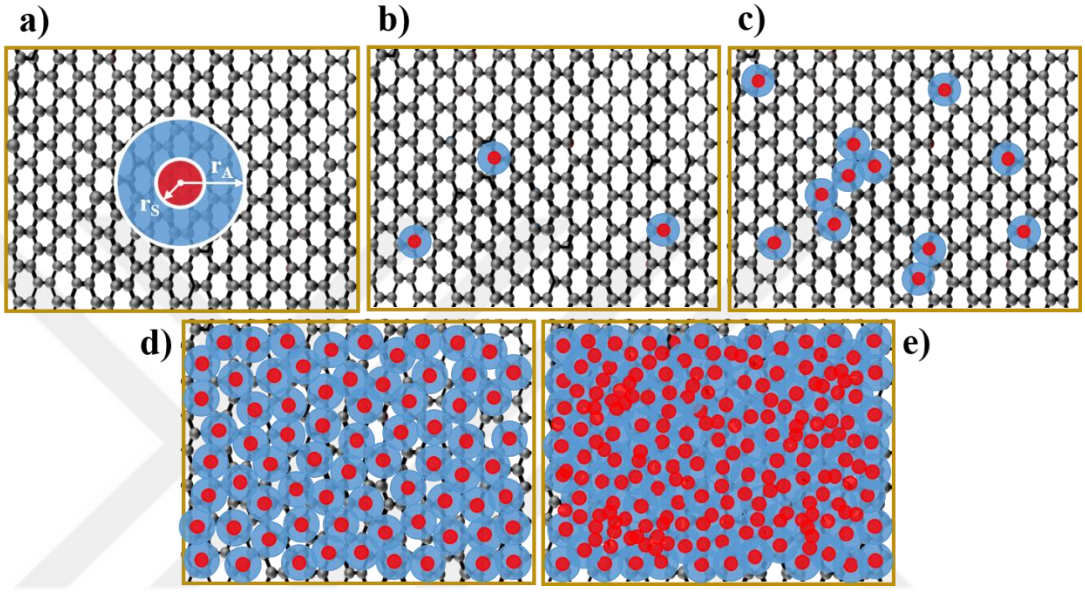

Figure 9 a) Definition of "active area" (blue region) and "structurally disordered area" (red region) cause by Ar^+ bombardment. r_A and r_S are the radii of activated and structurally disordered areas, respectively. b-e) evolution of randomly chosen impact points on single-layer graphene for various defect concentration of b) 10^{11} Ar^+/cm^2 c) 10^{12} Ar^+/cm^2 d) 10^{13} Ar^+/cm^2 e) 10^{14} Ar^+/cm^2 . Adapted from [77].

2.5.2.3. 2D Band

The 2D peak is known as an overtone of the D peak, however, it is not related to the physical defects of the graphene itself. It is located at ~2700 cm^{-1} (Figure 6) and appears due to second order of zone-boundary phonons [72]. Figure 10 represents the electron-hole creation and electron-phonon scattering process resulting this band.

Different features of above mentioned bands have been used to characterize properties of single and multi-layer graphene. For example, while the 2D peak in graphite is asymmetric and wider, it is narrow and symmetric in graphene. This is due to the fact that other vibrational

modes in the 2D peak are more active in graphite. So, it can be expected that higher quality graphene will have less Full Width at Half Maximum of 2D peak ($FWHM_{2D}$).

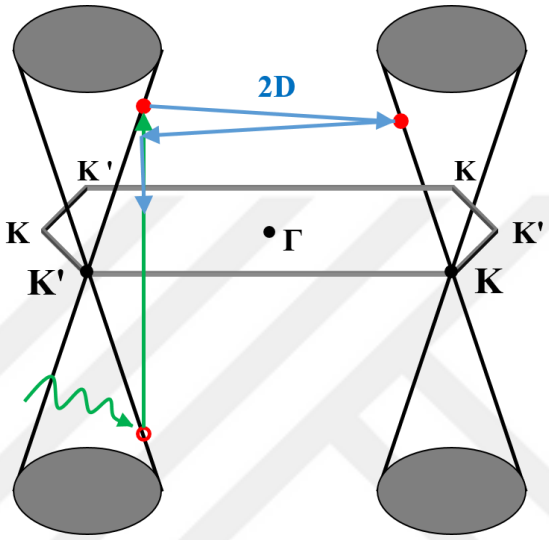

Figure 10 Schematic representation of the electronic dispersion near the fermi level at the K, K' points in the hexagonal Brillouin zone of graphene. The electron-hole pair generated by incident light (green arrow) and electron-phonon scattering processes resulting 2D band are shown.

A general comparison between Raman spectra of graphene and graphite reveals that from intensity point of view, the 2D peak of graphite is much smaller than the G peak of it, however, in graphene the 2D peak is sharper than the G peak, reaching to more than 3 times of the intensity of G peak in single-layer graphene [78]. Consequently, the 2D to G intensity ratio (I_{2D}/I_G) can be used to determine the number of the layers in few layer graphene, but one should consider that some processes like doping [79], [80] or introduction of new defects to the graphene [81] can change this ratio. So the accurate interpretation of I_{2D}/I_G can be done, only by controlling other characteristic features of graphene Raman spectrum, simultaneously.

In addition to $FWHM_{2D}$ and I_{2D}/I_G, shape of this peak has been also used to characterize number of layers in graphene samples. As it can be seen in Figure 11a and Figure 11b, the

line shape of 2D peak depends on the number of layers and while in single layer graphene the 2D band consists of only one peak, bi-layer graphene has a 4-peak 2D band. This phenomena can be explained by the special electronic structure of bi-layer graphene, which consists of two conduction and two valence band regions [82], as shown in Figure 11d-g. The possible double resonance Raman processes that give rise to the four 2D band, are shown in this figure. The Figure 11d represents the absorption and scattering process of highest frequency 2D peak and Figure 11f shows the lowest frequency peak [76]. The double resonance processes for tri-layer graphene reaches to 15 possibilities, however very small difference between their frequencies makes it a demanding task to identify these peaks [82]. This status is obvious in Figure 11c.

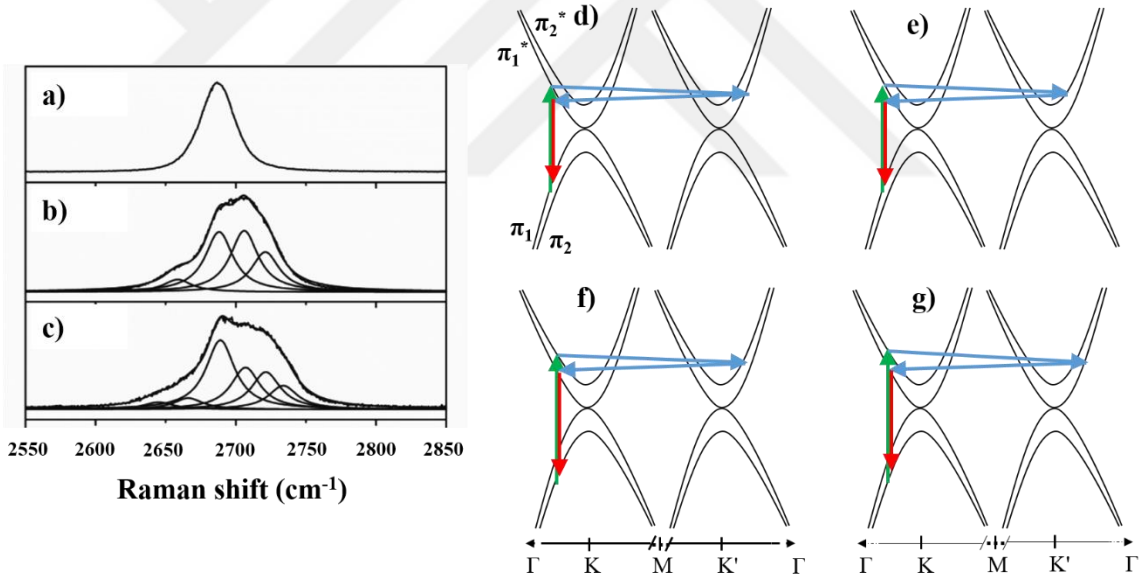

Figure 11 The differences for 2D band of a) mono-layer, b) bi-layer and c) tri-layer graphene, adapted from [76]. d-g) Scattering processes which result in having four different peaks for 2D band of bi-layer graphene shown in (b).

2.5.3. Raman Characterization of Graphene

Raman spectra of graphene samples on Cu substrates were measured by Renishaw inVia Raman microscope using 100% laser power at wavelength of 633 nm with beam size of 2

μm. The same device was used to characterize graphene samples on SiO_2/Si substrate, however in this case 10% laser power at wavelength of 532nm hit the sample. To verify the presence of nitrogen in the structure of graphene, Raman spectra were taken both before and after nitrogen plasma treatment.

Due to the non-homogenous nature of centimeter scale graphene samples prepared in this study, a single Raman spectrum which contains information about a sub micro meter area of graphene cannot represent the overall structure. A comprehensive Raman investigation of graphene films was done by taking multiple spectra from different parts of a single sample. These results are presented using statistical box charts in Chapter 3 and Chapter 4. There are some fundamental statistical terms, such as mean, median and quartile, which are beneficial to have a better understanding from those charts. While mean is the average of all data, median is the middle number in a sequence of them. In the sequence order of data, three points can always be found in a way to divide all of the data to four groups containing equal number of data. Each of these groups is known as a quartile.

In addition to multiple spots Raman spectroscopy characterizations, Raman maps were taken from some samples. In this case, the distance between spots was 0.5 μm and Raman spectra of these points in 1600 μm^2 were collected. These spectra were further analyzed to obtain color maps based on I_{2D}/I_G and I_D/I_G.

2.6. X-ray Photoelectron Spectroscopy (XPS)

2.6.1. Theory of XPS

Most forms of matter present in the solid or liquid phase exhibit a surface layer that is different from that of the underlying material. There might be a chemical (composition or speciation) and/or structural (differences in bond angles or bond lengths) origin for this difference. How a material is perceived by the outside world thus depends on the form of the outer layer. Additionally, the great improvement in technology of thin films has increased attention to them in both scientific and technological areas. If the surface composition and

speciation can be characterized, the manner in which the respective solid, liquid or thin film interacts with its surroundings can more effectively be understood. This, then, introduces the possibility of modifying (tailoring) these properties as desired.

Photoemission spectroscopy is based on the photoelectric effect, which in its simplest form describes a single step process in which an electron initially bound to an atom/ion is ejected by a photon. Since photons are a massless (zero rest mass) and chargeless package of energy, these are annihilated during photon–electron interaction with complete energy transfer occurring. If this energy is sufficient, it will result in the emission of the electron from the atom/ion as well as the solid. The kinetic energy (E_k) that remains on the emitted electron is the quantity measured. This is useful since this is of a discrete nature and is a function of the electron binding energy (E_b) [83]. The number of photoelectrons depends on the light intensity, and the energy of the electrons on the wavelength of the light.

XPS has become one of the most favorite surface characterization methods among scientists in last decade. A technique becomes surface-sensitive if the radiation or particles to be detected travel no more than a few atomic distances through the solid. The diagram in Figure 12 shows that the mean free path, λ, of electrons in elemental solids depends on the kinetic energy, but is limited to less than 1–2 nm for kinetic energies in the range 15 to 1000 eV [84]. Optimum surface sensitivity ($\lambda \sim 0.5$ nm) is achieved with electrons have kinetic energies in the range of 50 to 250 eV, where almost half of the photoelectrons come from the outermost layer.

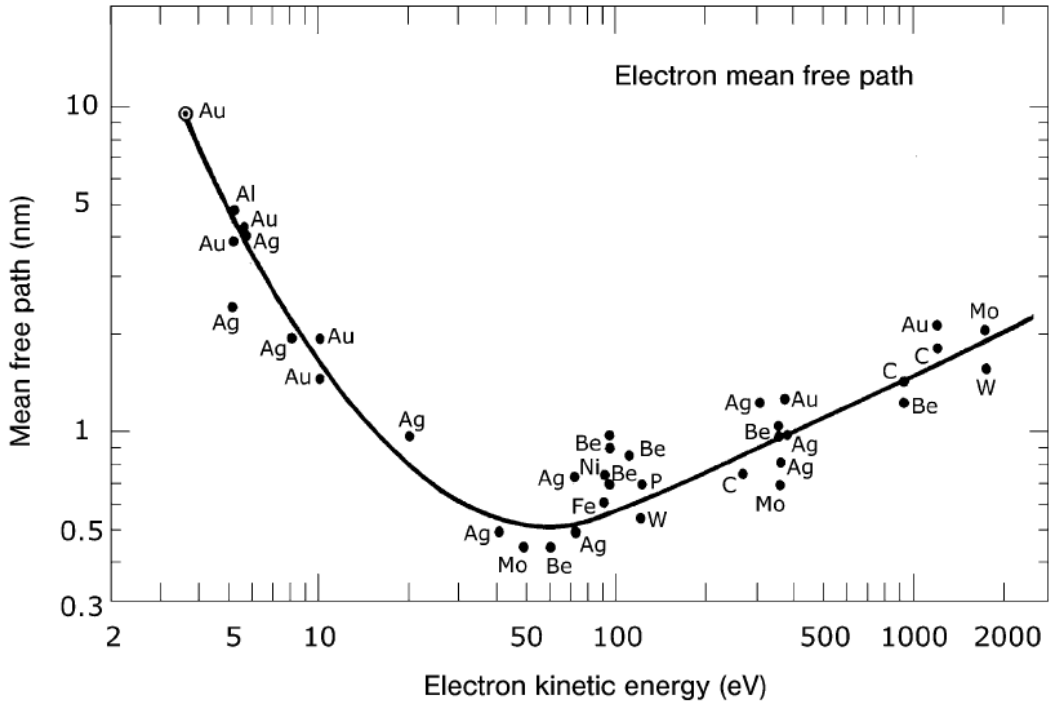

Figure 12 The mean free path of an electron depends on its kinetic energy, and determines how much surface information it carries. Optimum surface sensitivity is obtained with electrons in the 25 to 200 eV range. (Adapted from [84])

As mentioned above, XPS is based on the photoelectric effect, whereby an atom absorbs a photon of energy, hν, after which a core or valence electron with binding energy E_b is ejected with kinetic energy, E_k:

$$E_k = h\nu - E_b - \varphi \qquad \text{Equation 7}$$

Where:

E_k is the kinetic energy of the photoelectron;

h is the Planck's constant;

ν is the frequency of the exciting radiation;

E_b is the binding energy of the photoelectron with respect to the Fermi level of the sample;

Φ is the work function difference between the sample and the spectrometer

Mg Kα (hν=1253.6 eV) and Al Kα (hν=1486.3 eV) are usually used as X-ray sources. The XPS spectrum, however, is usually a plot of N(E) versus E_k, or, more often, versus the E_b. It is noteworthy that the value obtained from XPS is not equal to the binding energy in the ground state atom; that is, the introduction of a core hole during photoemission effectively alters binding energy. Values from that exhibited by a ground-state atom/ion, albeit by a small amount. This effect, referred to as a final state effect, which can be divided into two groups, "core-hole induced polarization" and "core-hole induced rearrangement". Core hole induced polarization is an instantaneous effect that results from the removal of a spinning charge (the photoelectron) from an atom/ion. This not only results in an electrostatic effect but also in a magnetic effect. These can influence the recorded binding energy in a number of different ways. Rearrangement effects originated from the energy transfer associated with the dissipation of the core hole produced during the photoelectron emission process. Since this and any subsequent electronic rearrangement can occur within the timescale of photoelectron emission, these can introduce new rearrangement-specific spectral features like satellite peaks, photoelectron peaks asymmetry, plasmon loss peaks and Auger electron peaks.

During the process of analyzing XPS data ones should be careful about Auger effect which is occurred as a result of de-excitation process that follow photoelectron emission. Auger electron emission is observed for all elements containing three or more electrons (Li–U) with the emission probability being a function of Z. The first electron of three electrons needed for Auger process represents the photoelectron. The second and third electrons remove the energy associated with the core hole; that is, the second electron drops down from some level of lesser binding energy to fill the core hole and the third electron removes the energy associated with this transition.

Analysis is usually carried out by first collecting energy spectra over all accessible energies and then concentrating on particular photoelectron signals. This ensures that all

elements are accounted during quantification and that the data are collected in a time-effective manner.

Photoelectron peaks are labeled according to the quantum numbers of the level from which the electron originates. An electron with orbital momentum *l* (0, 1, 2, 3 … indicated as s, p, d, f . . .) and spin momentum *s*, has a total momentum j = *l* + *s*. As the spin may be either up (*s* =1/2) or down (*s* = -1/2), each level with $l \geq 1$ has two sublevels, with an energy difference called the spin-orbit splitting.

Spin-orbit splittings as well as binding energies of a particular electron level increase with increasing atomic number. The intensity ratio of the two peaks of a spin-orbit doublet is determined by the multiplicity of the corresponding levels, equal to 2j + 1. Hence, the intensity ratio of the j = 7/2 and j = 5/2 components of the Pt 4f doublet is 8:6, and that of the 5/2 and 3/2 peaks of the 4d doublet is 6:4, etc. Thus, photoelectron peaks from core levels come in pairs (doublets) except for s levels, which give a single peak.

The popularity of XPS is because of its ability to identify and quantify the elemental composition of the outer 10 nm or less of any solid surface with all elements from Li–U detectable. Surface specificity arises from the limited flight path an electron has within a solid before it loses some fraction of its energy, which is normally less than 10 nm. However, X-rays can penetrate micrometers below the surface. If energy is lost, the signal will disappear within the spectral background. This occurs for almost all photoelectrons produced from atoms/ions situated at some depth greater than ~10 nm below the surface. All of these depth limitations are on the assumption that the element of interest exists at > 0.05 atomic present. It can also reveal the chemical environment where the respective element exists in, that is, the speciation of the respective elements observed. Finally, researchers can obtain the above information with relative ease and minimal sample preparation [83].

Sensitivity of XPS is primarily a function of the photoelectron cross section and the spectral background level. The photoelectron cross section describes the yield of electrons

produced as a function of the impacting photon energy. Indeed, the low photoelectron cross sections from H and He under X-ray irradiation are the primary reason why these elements are not detectable when present within solids. The spectral background arises from a number of sources with the most prevalent being inelastic scattering of electrons. The non-discrete energy loss resulting from inelastic scattering (energy lost by electrons still within the solid to its surroundings) produces a broad background to the lower kinetic energy side of the peak of interest. The ambient pressure, or more precisely the vacuum under which the analysis is carried out, can also affect sensitivity since this controls the density of molecules in the gas phase and, thus, the flight path of any photoelectrons emanating from the surface. Contaminant overlays also form within analysis timescales if the pressure under which the analysis is being carried out is too high.

When electrons or other charged particles moving at relativistic speeds are forced by magnetic fields to follow curved trajectories they emit electromagnetic radiation in the direction of their motion, known as synchrotron radiation. Such radiation is extremely intense and extends over a broad energy range from the infrared through the visible and ultraviolet, into the soft and hard x-ray regions of the electromagnetic spectrum [85]. Recent progress of x-ray undulators at third-generation synchrotron light sources enables delivery of unprecedented high photon flux as well as high flux density. In order to have a more precise investigation on the samples prepared in this project an XPS device which was fed by X-ray coming from synchrotron was also used.

2.6.2. XPS Characterization of Graphene Samples

Atomic composition of the samples on both substrates before and after nitrogen doping was characterized by Thermo K-alpha X-ray photoelectron spectroscopy system. Nitrogen, carbon and survey spectra of different spots on each sample were analyzed. Additionally, in order to make sure about any residual of copper after transfer and oxidation during transfer or doping, oxygen and copper high resolution spectra were also obtained.

2.7. Atomic Force Microscope (AFM)

2.7.1. Theory of AFM

In AFM a sharp tip, typically made of silicon or silicon nitride, approaches the surface of the sample. This tip is mounted on a cantilever which is connected to a piezo oscillator. In addition, a laser beam hits the back side of the cantilever in a way that the reflected beam goes directly to the center of a quadrant photo diode. During the measurement, the oscillator moves the cantilever up and down. When the tip reaches to the surface of the sample it will be pulled towards surface, due to different kinds of interaction between them (Van der Waals or electrostatic if the tip is coated with cobalt or etc.). In this situation the cantilever will be deflected and as a result, the laser beam will no longer hit the center of photo diode, which leads to different signals in each of the 4 parts of the detector. The calibration of this signal variation helps to detect the position of the tip and the amount of deflection of the cantilever, which is a sign of the strength of the above mentioned attraction between the tip and the surface [86].

Since 1986 that G. Binnig and C. F. Quate proposed the very first design of AFM [87], different modes of it have developed to modify the device in a suitable way for wide range of samples and characterization of various properties of them. Figure 13 depicts three main categories of these modes, which in general are classified as contact mode, intermittent contact mode and non-contact mode, on the curve of force of interaction between the tip and the surface versus the distance between them. As it can be seen, in the contact mode which operates in the repulsive region of the force-distance curve, the tip touched the surface. This mode gives comprehensive and detailed information about the topography however due to the contact between tip and surface, number of runs that the tip can perform is limited and after some time it gets blunt. An alternative method is non-contact mode, where the tip approached the surface but do not touch it. Here the frequency of piezo by which it oscillates the cantilever is an important factor. Due to the interaction of the tip with surface of the sample, whenever it feels the surface, there will be a delay for the cantilever to come back to

its initial position, as a result there will be a phase shift in the detector which is used to generate the final image. Intermittent contact mode which is also known as tapping mode starts at the attractive region of force –distance curve and continues till the tip moves into the sample and then comes out. This method is mainly used to study stiffness of surface [88]. More modifications of the tip and its operation distance result in other modes such as force modulation, lift mode, chemical force microscope, etc.

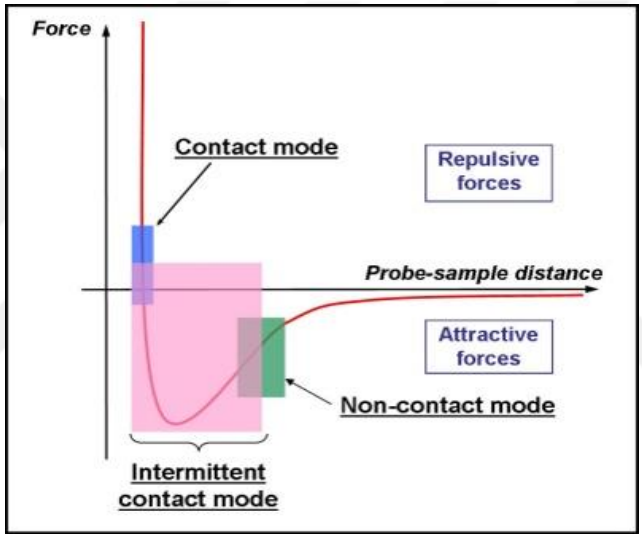

Figure 13 Force-distance for a tip reaching to the surface. The three main modes of AFM are shown as contact mode, intermittent contact mode and non-contact mode.

2.7.2. AFM Characterizations Graphene Samples

The AFM characterization of pristine and N doped graphene samples on SiO_2/Si substrate has done by a Bruker "dimension icon" system. The images were obtained in non-contact mode using Bruker "scanasyst-air" tips. The main goal was to investigate topography change before and after doping nitrogen in the structure of graphene.

Chapter 3
The Effect of Growth Parameters on the Quality of Graphene

Raman spectroscopy is a powerful technique for determining the number of layers and quality of graphene grown on copper foils and also transferred onto SiO_2/Si substrates, for this reason, spectral features could be used to investigate the effect of different growth parameters. Gas composition, total reactor pressure, heating rate, hydrogen treatment, synthesis temperatures, and synthesis duration were the parameters under investigation. Not only these parameters individually play an important role in the quality of graphene, but also their correlation make an impact. In this section, the effects of the synthesis parameters on the graphene quality will be emphasized individually.

3.1 Effect of Flow Rate of Methane in Low Pressure Synthesized Graphene

Previous studies have shown that the effect of methane flow rate on synthesis of graphene by CVD method can be investigated directly and indirectly. In a direct point of view, high flow rates of methane increase its concentration near the surface which results in growth of multilayer graphene on Cu [55]. On the other hand, lowering flow rate of methane will decrease carbon adsorbates on the copper and as a result there will be lower number of graphene nucleation sites. This effect can assist to increase uniformity of the graphene by reducing its growth rate [89]. The indirect effect of methane flow rate can be seen when we compare its partial pressure with the partial pressure of hydrogen. As it has discussed in the Chapter 2, hydrogen has dual effect; it plays a co-catalyst role in formation of carbon species and also it controls graphene grain shapes and size by etching it. Vlassiouk et al [55], have shown that dehydrogenation of methane is a rate limiting factor and presence of H_2 helps to

drive this reaction. As a consequence, there will be no graphene film in very high partial pressures of methane because copper itself cannot provide enough energy for methane activation.

Four samples were synthesized using different flow rates of methane in order to investigate the effect of this parameter and modify it. These samples were prepared by 5, 10, 20 and 30 sccm of methane, respectively. The Raman spectra obtained from different parts of these samples showed that despite the samples synthesized with 10, 20 and 30 sccm of methane, the 5 sccm flow rate of methane was not enough to synthesis an integrated film and it contained graphene islands. This result was approved by optical microscope images [70]. Figure 14 shows OM images of the samples prepared by 20 sccm (Figure 14a) and 5 sccm (Figure 14b) of methane. The samples were held at 200 ^{o}C for 10 minutes in order to have better contrast in the images. During this process that we named as "baking", the parts of the copper substrate which were not covered with graphene oxidized and appeared as reddish parts in OM images. The results showed high concentration of these reddish parts on the samples prepared by 5 sccm of methane while the other samples had more homogenous images. The darker parts in Figure 14a can be due to the colorless nature of graphene which causes to see the underneath substrate more clearly.

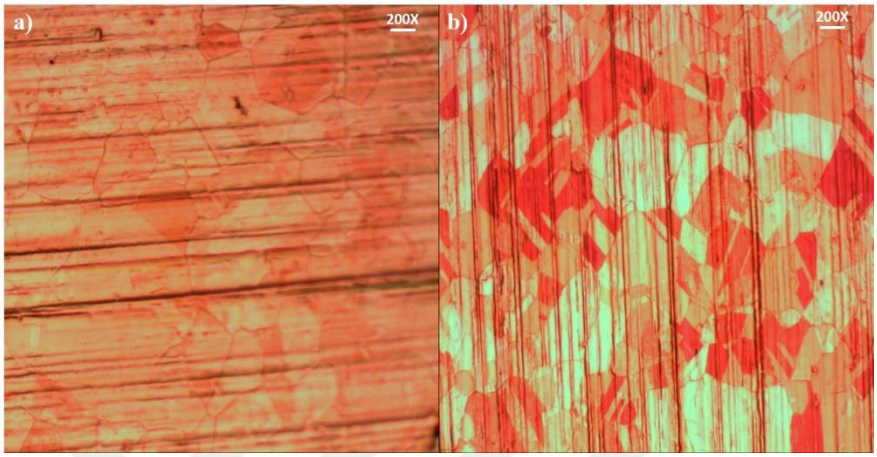

Figure 14 OM images of graphene sample on copper, prepared with a) 20 and b) 5 sccm, after baking them at 200 ^{o}C for 10 min. All the other growth parameters were the same in both samples. The magnification of images is shown in top right corner of them.

As it can be seen in Figure 15, the other three samples had graphene with different qualities. While all of the samples have the three main fingerprint peaks of graphene, (D, G and 2D bands at ~1335 cm^{-1}, ~1590 cm^{-1} and ~2670 cm^{-1}, respectively), the I_{2D}/I_G ratios (which is an indication of number of layers) are 1.51, 1.37 and 0.51 for the samples prepared by 10, 20 and 30 sccm of methane, respectively. This shows that while supplied methane amount for the sample prepared with 5 sccm flow rate was not enough to synthesize an integrated film, this amount is surplus when the copper substrate is subjected to 30 sccm of methane. As a result, the sample with highest flow rate of methane (30 sccm) had more than 10 layers of graphene, while the samples prepared with 10 and 20 sccm of methane had less numbers of layers. The density of defects is the other key factor, which can be evaluated by studying the I_D/I_G ratio or $FWHM_{2D}$. The higher these two quantities are the more defects graphene has. Among above mentioned three samples the 20 sccm of methane resulted in a sample with the lowest I_D/I_G ratio. So 20 sccm of methane is taken as the optimum flow rate to grow multi-layered graphene with low number of defects at total pressure of ~ 0.5 Torr.

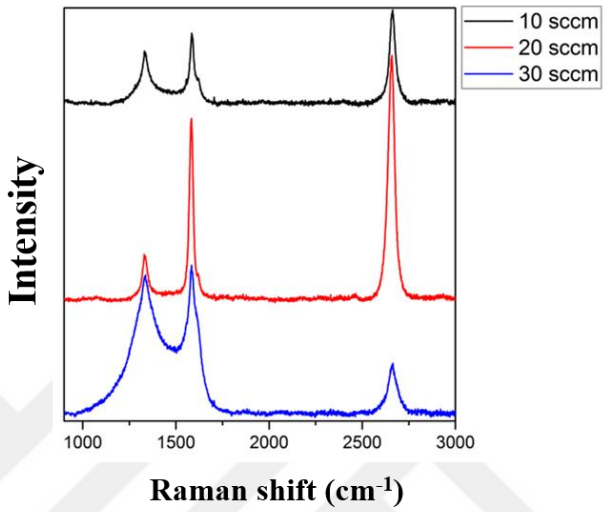

Figure 15 Raman spectra of graphene samples prepared with different flow rates of methane (10, 20 and 30 sccm), the samples were heated up to 900 ^{o}C with heating rate of 5 ^{o}C/min to be treated with H_2 under 100 sccm of Ar and 20 sccm of hydrogen for 30 minutes. The growth was done at the same temperature for 45 minutes. Flow rates of Ar and H_2 were the same as hydrogen treatment step during the growth. The whole synthesis process was done at ~0.5 Torr.

3.2 Effect of Growth Time on Low Pressure Synthesized Graphene

In order to investigate the effect of the growth time, graphene was grown by subjecting it to methane at 900 ^{o}C for 45, 30 and 15 minutes, respectively. Figure 16 shows Raman spectra of these graphene samples on Cu obtained by 633 nm wavelength laser. It is obvious that from thickness point of view, all samples are multi-layered graphene, however their qualities are different. Intensity ratios between D band and G bands are 0.22, 0.69 and 0.73 for the samples with growth duration of 45, 30 and 15 minutes, respectively. As a consequence, among these three studied samples, the longer the growth time the lower defect density in the sample.

Another main characteristic point that can be extracted from Figure 16, is the total area of graphene sheet in different growth times. Higher total intensity of sp^2 carbon peaks (2D and G bands) is a sign of more graphene on the Cu substrate. Since the number of layers in the samples showed in Figure 16 do not vary too much, the higher total intensity of the sample prepared for 45 minutes reveals that this film is more extended in comparison with the others. The majority of the disorders in pristine graphene samples are vacancy defects. Consequently, it can be expected that a sample with more vacancy shows higher I_D/I_G ratio and lower total graphene intensity. Such trend can be obviously found in Figure 16, where higher exposure time to the methane flow is resulted in low vacancy density and larger graphene sheets.

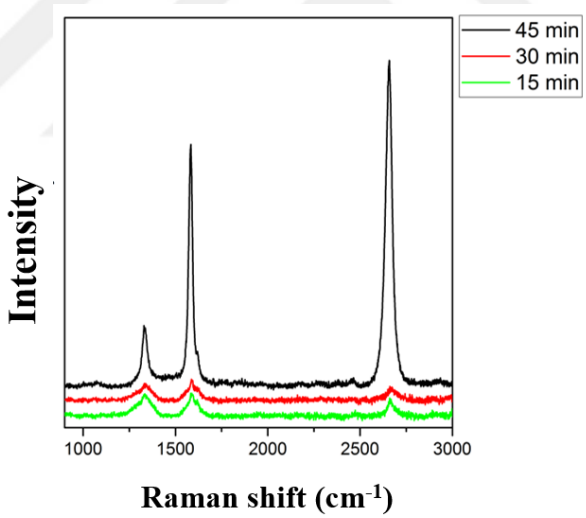

Figure 16 Raman spectra of graphene samples prepared with different growth times (15, 30 and 45 minutes), the samples were heated up to 900 ºC with heating rate of 5 ºC/min to be treated with H_2 under 100 sccm of Ar and 20 sccm of hydrogen for 30 minutes. The growth was done at the same temperature. 20 sccm of methane were added to Ar and H_2 during the growth. The whole synthesis process was done at ~0.5 Torr.

3.3 Effect of Synthesis Temperature

The other factor which was necessary to be modified is synthesis temperature. Regmi et al. investigated the effect of temperature on graphene quality by fixing all synthesis parameters except temperature over the interval 600-1000 ^{o}C. According to their results, no graphene growth occurred below 850 ^{o}C. They also showed that the samples synthesized at 900 ^{o}C were consisted of graphene multi-layer islands. However, the samples prepared at 950 and 1000 ^{o}C under the same growth parameters as the previous ones, were almost single layer graphene, [52]. Higher temperature means more supplied energy for hydrocarbon decomposition and catalyst activation, however, copper substrate was evaporated at temperatures higher than 900 ^{o}C due to the low operation pressure of our CVD system. On the other hand, from energy consumption point of view it is essential to perform the synthesis at the lowest possible temperature. In order to reach this goal, a sample was prepared at 850 ^{o}C while the other synthesis factors were the same as previously modified sample. Figure 17 compares the Raman spectra of these two samples. It can be seen that all of the main Raman features of graphene (I_{2D}/I_G and I_D/I_G ratio and $FWHM_{2D}$) for the sample prepared at higher temperature are better than the one synthesized at 850 ^{o}C. As a result, 900 ^{o}C was chosen as the optimum temperature to synthesis graphene at 0.5 Torr in our CVD system. The combination of this results and literature review suggests that lowering the growth temperature decreases growth rate of the first layer in comparison with the growth rate of next ones, which results in having non-integrated multi layers flakes over copper substrate.

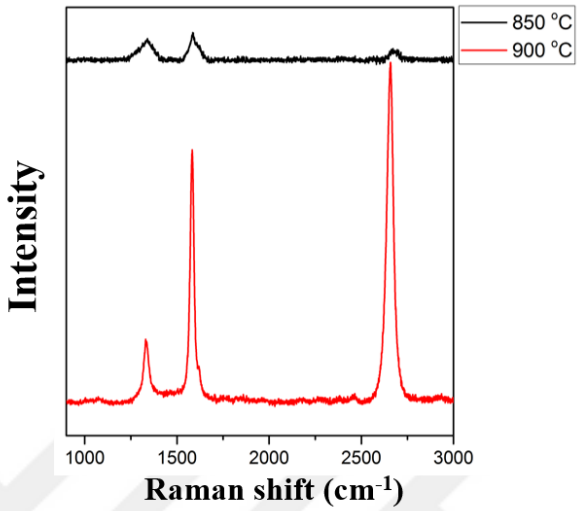

Figure 17 Raman spectra of graphene samples prepared with different synthesis temperature (850 and 900 °C), the samples were heated up to 900 °C with heating rate of 5 °C/min to be treated with H_2 under 100 sccm of Ar and 20 sccm of hydrogen for 30 minutes. The growth duration was set to be 45 minutes. 20 sccm of methane was added to Ar and H_2 during the growth. The whole synthesis process was done at ~0.5 Torr.

3.4 Effect of Pressure

While our initial graphene growth attempts were done at LPCVD regime (≤ 0.5 Torr), we decided to synthesize graphene at higher pressures in order to identify the effect of the total pressure. Three samples were synthesized at 4, 5 and 6 Torr, respectively. All other synthesis parameters were the same as the LPCVD samples. Some groups like Vlassiouk et al. [90] have claimed that LPCVD and HPCVD samples have to investigate separately because the dehydrogenation process of carbon precursor is not the same. They also showed that the limiting factors for graphene growth at HPCVD are different than the ones at LPCVD samples. However there are still vast number of studies without this classification. Bhaviripudi et al. [91] have shown that higher concentration of methane near the surface of copper at high pressures has two main effects on properties of graphene. First, it causes to

have graphene samples with higher number of layers and secondly, the nucleation density increases due to lower H_2 concentration on the surface, which results at higher grain boundary density. Consequently, there will be more defect points on graphene and the Raman spectrum of such a sample is expected to have higher D peak intensity. This effect is the same as the one expected for high flow rates of methane, however the lack of sufficient amount of methane due to the low flow rate cannot replaced by increasing pressure, because in addition to the change in concentration of methane the sticking probability of them is also changed with any alter in flow rate. Figure 18 shows the results for number of layers of the samples synthesized at 4, 5 and 6 Torr total pressure. I_{2D}/I_G decreased from 2.67 to 1.99 and 1.59 by increasing the pressure. However all of these samples had lower number of layers in comparison with the LPCVD sample (I_{2D}/I_G = 1.37). In contrast with I_{2D}/I_G trend, the intensity ration of D over G peaks didn't not show a significant change (0.22, 0.21, 0.22 and 0.18 for the samples prepared at 0.5, 4, 5 and 6 Torr respectively), which can be attributed to the high H_2 flow rate (H_2/CH_4 = 2.5). As a consequence, synthesis of graphene with previously chosen parameters at 4 Torr results in a two to three layer graphene with good quality. Using 4 Torr total pressure made it feasible to perform hydrogen treatment step at 950 ^oC for longer time (90 minutes) without any evaporation of Cu. The higher temperature and duration of hydrogen treatment step result is a copper foil with larger flat plateaus which provide catalyst sites to grow more homogeneous graphene.

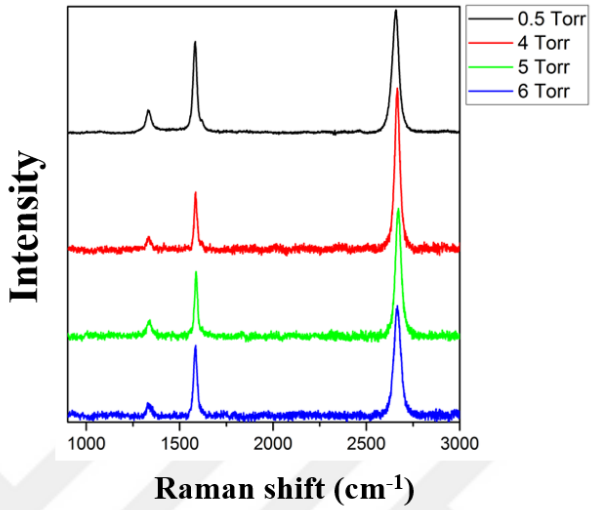

Figure 18 Raman spectra of graphene samples prepared in different total pressures (0.5, 4, 5 and 6 Torr), the samples were heated up to 900 ºC with heating rate of 5 ºC/min to be treated with H_2 under 100 sccm of Ar and 20 sccm of hydrogen for 30 minutes. The graphene growth was done at the same temperature for 45 minutes. 20 sccm of methane was added to Ar and H_2 during the growth.

Due to the fact that different spots on a graphene sample have not exactly the same spectral features, Raman spectra from 40 different points on each of modified samples with LPCVD and HPCVD regimes were taken in order to have a more precise investigation on samples prepared at low and high pressures. Figure 19 depicts the four different quartiles in I_{2D}/I_G (Figure 19a) and $FWHM_{2D}$ (Figure 19b) ranges as well as the mean and the median of these results. It is obvious that all of the points on HPCVD sample have I_{2D}/I_G higher than the mean I_{2D}/I_G of LPCVD graphene and also almost 70% of the points on HPCVD have $FWHM_{2D}$ lower than the mean of the same quantity for LPCVD. In the other words, synthesis of graphene at 4 Torr results in a sample with lower number of layers and lower density of defects in comparison with the sample prepared at 0.5 Torr.

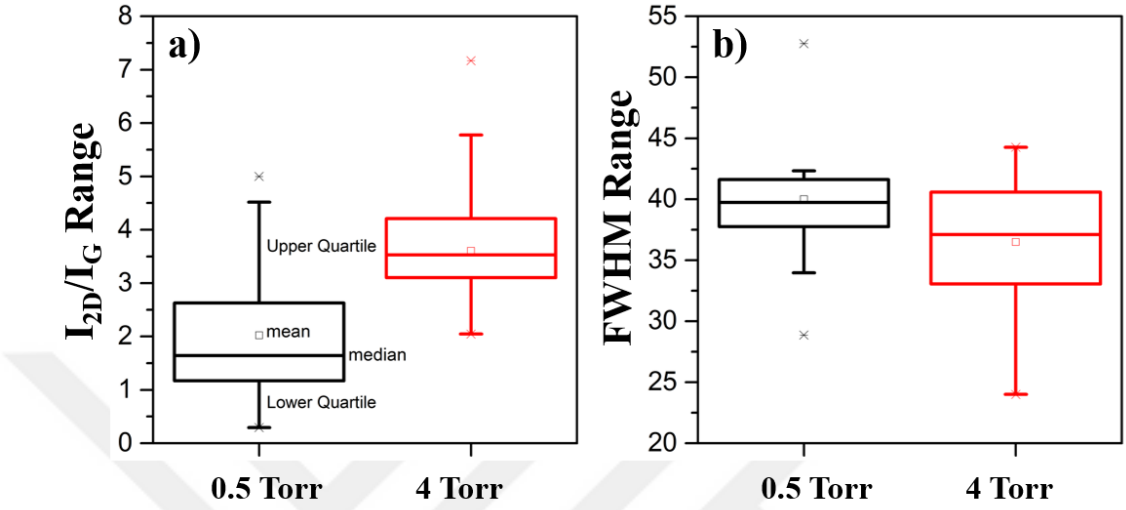

Figure 19 Box charts showing a) I_{2D}/I_G range, b) $FWHM_{2D}$ range for 40 spots on the samples prepared at 0.5 and 4 Torr

3.5 Effect of Heating Rate:

One of the most important factors that determines the properties of graphene grown by CVD method is the properties of the copper substrate. Crystal structure of polycrystalline Cu as well as its roughness can affect the graphene [92], [93]. Wood et al. have shown that while monolayer graphene with large grain size can easily grow on Cu(111), higher-index facets provides a condition to synthesis of multi-layered graphene with high defect density and high grain boundary density [92]. In addition, Luo et al. have concluded that flat surface morphology is a crucial factor to improve homogeneity and quality of graphene [93]. Figure 20a, shows Raman spectra of two graphene samples synthesized at 900 ^oC using 20, 100 and 20 sccm of Ar, H_2 and CH_4, respectively. The growth time and total pressure were set to be 45 minutes and 4 Torr. Both samples were treated under hydrogen atmosphere at 950 ^oC, prior to the growth of graphene. The heating rate of Cu substrate to reach to the hydrogen treatment and synthesis temperature was the only difference between these two samples, where for one of them the initially set heating rate (5 ^oC/min) was applied but for the second

one this amount was doubled. The intensity ratio of 2D over G and D over G for fast heated sample, were 1.88 and 0.34, respectively. There was a significant improve in the same quantities for the other sample, where I_{2D}/I_G was equal to 2.67 and I_D/I_G was equal to 0.21. It seems that providing longer time for the copper substrate at elevated temperatures helped it to have a surface with lower roughness and higher concentration of facets on which less number of layers of graphene grow. Figure 20b, and Figure 20c confirm the same conclusions by showing box charts of I_{2D}/I_G and $FWHM_{2D}$ for 30 different spots on each of the samples. However, it seems that more deeper and precise studies need to be done on the effect of this parameter specially for polycrystalline copper substrates where presence of different planes of copper and their grain boundaries can make the growth of graphene complicated.

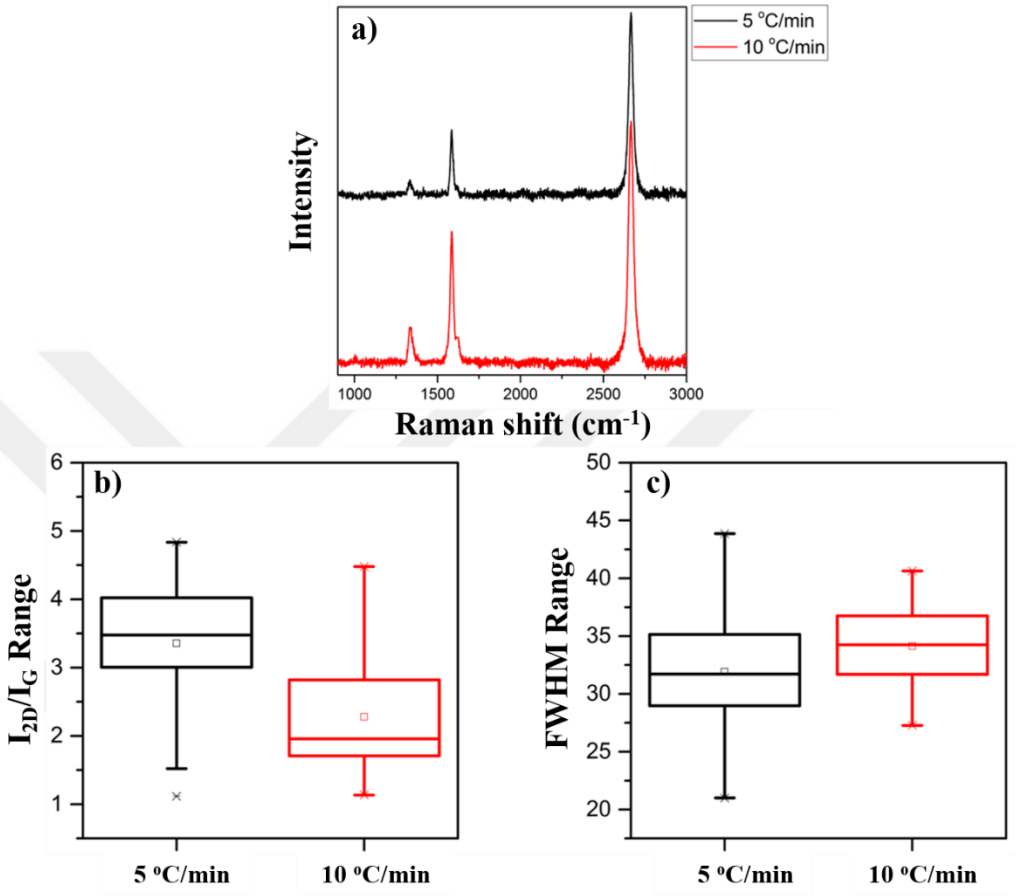

Figure 20 a) Raman spectra and box charts for b) I_{2D}/I_G and c) $FWHM_{2D}$, of graphene samples prepared with different heating rate (5 and 10 °C/min). The samples were heated up to 950 °C to be treated with H_2 under 100 sccm of Ar and 20 sccm of hydrogen for 90 minutes. The graphene growth was done at 900 °C for 45 minutes. 20 sccm of methane was added to Ar and H_2 during the growth. The whole synthesis process was done at ~4 Torr.

3.6 Effect of Flow Rate of Methane on HPCVD Graphene

Due to the high impact of methane flow rate on the features of graphene synthesized by CVD, its effect on HPCVD samples was studied as well. Since Raman spectra obtained from

the sample prepared with 20 sccm of methane under HPCVD conditions was showing a two or three layer graphene with low defect density, we focused on synthesizing samples with lower methane flow rates. Figure 21a shows Raman spectra of the previously modified graphene and a samples with the same parameters but lower flow rate of methane (10 sccm) on copper substrate. There was a significant increase in intensity ratio of 2D band over G band due to the less concentration of carbon on the surface and since, $I_{2D}/I_G = 4.96$, 10 sccm flow rate of methane was caused to produce a monolayer graphene. However, the most important difference between these two samples was the almost negligible D peak of the one with lower flow rate of methane which is in agreement with the results that Liu et al. have obtained [89]. Figure 21b and Figure 21c depict a better and more comprehensive view of above mentioned samples by showing the box charts of $FWHM_{2D}$ and I_{2D}/I_G of 50 different points on each sample. Figure 21b approves the improvement in the quality of graphene that was shown in Figure 21a. However, Figure 21c shows that in contrast with the result that was obtained from comparison of I_{2D}/I_G of the samples in Figure 21a, even 10 sccm of methane doesn't result in synthesis of completely homogenous monolayer graphene and almost 50% of the points had I_{2D}/I_G less than 2, which means there are some islands of second and even third layer on the first layer of graphene. On the other hand, comparison of red boxes with the black ones in each of the charts shows that the variation in I_{2D}/I_G and $FWHM_{2D}$ reduce with decrease of methane flow rate. It means that while it is really challenging to synthesize a homogenous large graphene sample without any post synthesis treatment, it is possible to decrease the order of variation in its quality by modification of growth parameters.

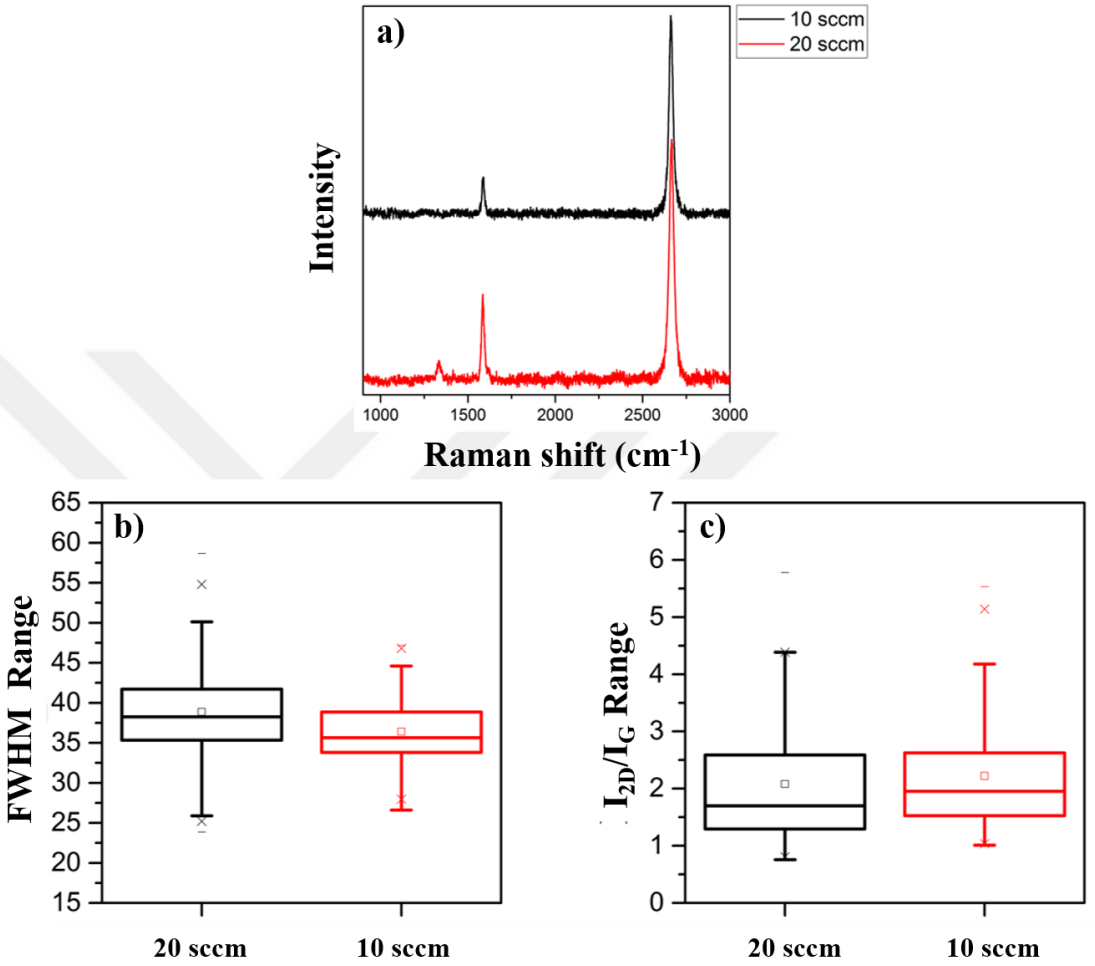

Figure 21 a) Raman spectra and box charts for b) FWHM of 2D band and c) I_{2D}/I_G, of graphene samples prepared with different flow rates of methane (10 and 20 sccm). The samples were heated up to 950 ºC with heating rate of 5 ºC/min to be treated with H_2 under 100 sccm of Ar and 20 sccm of hydrogen for 90 minutes. The growth was done at 900 ºC for 45 minutes. Flow rates of Ar and H_2 were the same as hydrogen treatment step during the growth. The whole synthesis process was done at ~4 Torr.

3.7 Investigation of the Defects Introduced to Graphene Structure During Transfer

After making sure about modification of all important factors and checking the reproducibility of best obtained sample, it was transferred onto SiO_2/Si substrate. The

discussion about best transfer method is out of scope of this thesis, however it was a main concern for this step of our project to study the amount of defects introduced to the graphene structure during transfer. Previously done quantification studies on Raman spectrum of graphene based materials [73], [94] have shown that I_D/I_G is proportional to λ^4, where λ is wavelength of excitation laser of Raman spectrometer. Since the laser wavelengths used to study graphene on copper and SiO_2/Si were 633 and 532 nm, respectively, it was expected that I_D/I_G values of graphene on SiO_2/Si become half of the same values obtained for graphene on Cu, if no defect was introduced during transfer. Figure 22, shows that the results didn't match the expectations meaning that in addition to the effect of changing wavelength of excitation laser, there was an increase in I_D/I_G, originating from introduction of new defects to the structure of graphene.

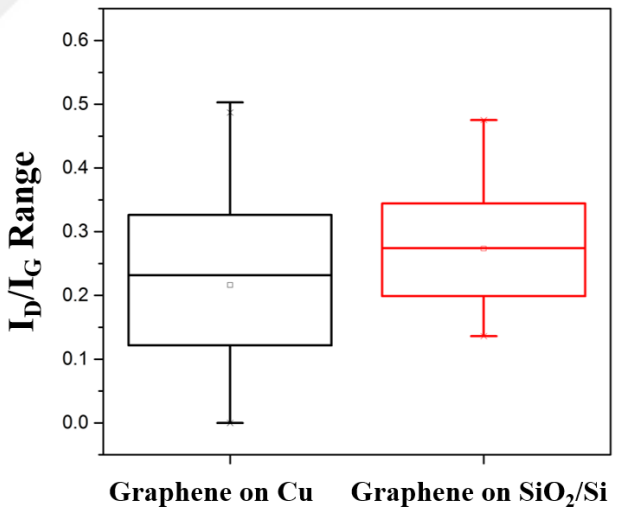

Figure 22 Box charts for I_D/I_G of graphene before and after transfer onto SiO_2/Si substrate

In addition to I_D/I_G, $FWHM_{2D}$ for different points on the same graphene sample before and after transfer was calculated as an indicator of amount of disorder introduced to the graphene structure during transfer process. Figure 23, shows the box charts corresponding to these results. It is confirming that due to the nature of wet chemistry method used for transferring the graphene, it is unavoidable to introduce some defects to the structure. However, the quality of graphene films after transfer is still in an acceptable grade to use this product in electrochemical applications.

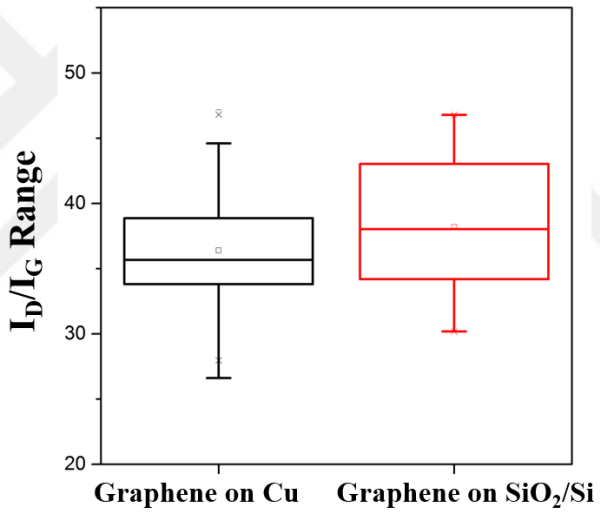

Figure 23 Box charts for $FWHM_{2D}$, of graphene sample before and after transfer onto SiO_2/Si

Chapter 4
Characterization of N Doped Graphene

As mentioned in section 2.2.3, the nitrogen atoms were doped into the graphene structure using nitrogen plasma. Nitrogen content, type of nitrogen atoms bonding to carbon atoms, effect of doping on the quality of graphene and some other issues regarding this process were investigated using Raman spectroscopy, XPS and AFM. In this chapter the results obtained from these characterizations will be reported and discussed.

4.1 Investigation on the Substrates to Doped Nitrogen into Graphene

Due to the complex nature of plasma environment, it was essential to choose the substrate on which graphene should be placed and exposed to the nitrogen plasma. There are three main features on Raman spectrum of N doped graphene which can be useful in order to study content of nitrogen in the graphene structure. All these features are shown in Figure 24, where Raman spectra of pristine and N doped graphene are presented. The first characteristic feature of N doped graphene is presence of D' band centered at around 1620 cm^{-1} which is known to be originated from intravalley double resonance scattering process [95]. In addition, a weak peak, D + D' band, appears for Raman spectrum of N doped graphene. This peak comes from the combination of different phonons with different momenta around K and Γ points [96]. Another main effect is the significant increase in the intensity of D band of N doped graphene in comparison with the pristine one. As previously discussed in section 2.3.2.2, D band is the result of a vibrational mode in sp^3 bonded carbon, which can be related to grain boundaries and nucleation sites. Low intensity of D band in the pristine graphene is

the sign of having mostly homogenous graphene with high degree of crystallinity, while intense D band in Raman spectrum of N doped graphene can correspond to the elastically scattered photo-excited electron created by the large number of nitrogen atoms embedded in the graphene lattice before emitting a phonon [97]. Evidently, $FWHM_{2D}$ changes in parallel with alter in intensity of D band. Finally, in addition to all these differences, intensity ratio of 2D band to G band is much lower for N doped graphene in comparison with the pristine sample.

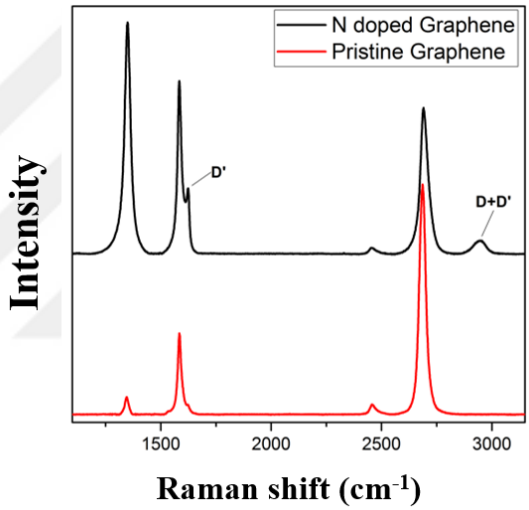

Figure 24 Raman spectra of pristine graphene and N doped graphene on SiO_2/Si substrate

In order to investigate possible difference in nitrogen content of graphene before and after transfer, we doped nitrogen in graphene structure on both copper and SiO_2/Si substrates and took Raman spectra from 50 different points on them. Figure 25 shows box charts of the results obtained from these Raman characterizations and compares a) $FWHM_{2D}$, b) intensity ratio of 2D band over G band and c) intensity ratio of D' band over G band for N doped graphene samples on Cu and SiO_2/Si substrates as well as pristine graphene on SiO_2/Si. The graphene samples which were exposed to nitrogen plasma before and after transfer are named

as SNT (Synthesis, Nitrogen doping and Transfer) and STN (Synthesis, Transfer and Nitrogen doping), respectively. Using the same naming system, the box chart of pristine graphene on SiO_2/Si substrate is shown with ST. The fact that almost all of the points on SNT and STN have larger $FWHM_{2D}$ with respect to ST sample is an evidence to synthesis of homogenous N doped graphene films. In addition, both N doped samples exhibit larger $I_{D'}/I_G$ in comparison with pristine graphene. This Raman feature approves the increase in the amount of graphene disorder after doping nitrogen. The same trend can be seen for I_{2D}/I_G.

In addition, it is obvious that above mentioned all three Raman disorder characteristic features are dominant for SNT in comparison with STN. This difference between SNT and STN can be explained by two plausible scenarios. The higher nitrogen concentration in SNT is the first possible reason to have larger D' band as well as broader 2D band. sp^3 disorders, vacancies and grain boundaries are the main types of defects in graphene. Doped nitrogen atoms acts as sp^3 defects because of a slight angle difference of C-N with respect to two dimensional sp^2 carbon structure of graphene. Doped nitrogen atoms connect to carbon atoms using vacancies, edges, grain boundaries or via substitutional process. Pyridinic and pyrrolic nitrogen creation is due to the above mentioned defects on pristine graphene, while graphitic configuration is a result of substitution. Since it has shown in section 3.7 that new defects were introduced to the graphene structure during transfer, the only possible reason to have larger I_D/I_G and $FWHM_{2D}$ for SNT in comparison with STN can be high concentration of graphitic nitrogen. The main parameter that can be effective in this process is the bond strength between graphene sheet and underlying substrate. Consequently, graphene should has strong bond with Cu which causes to weaken the C-C bonds in plane and facilitates the substitution of nitrogen. However, it is well-known that the interaction of graphene with both Cu and SiO_2/Si substrates is a weak physical one, which cannot alter C-C bond strength in a sensible scale. As the second possible scenario, the different features of SNT and STN can be seen as a result of more defects (rather than sp^3 defects due to N doping) on graphene.

Although, both SNT and STN were transferred with same method, however the presence of nitrogen in the structure of SNT could make it more sensitive to the wet chemical process. Consequently, while both of the samples had almost same concentration of nitrogen, the SNT sample contained higher amount of disorders introduced during transfer. Considering both, different factors that can affect intensity of 2D band and its FWHM and also complex nature of nitrogen plasma, more characterizations should be performed to make sure about main origin of these changes in Raman spectrum of nitrogen doped graphene. However even in the case of the second scenario, it is possible to dope nitrogen both before and after transfer and benefit from the disorders introduced during transfer. So since the main goal in this point was to choose nitrogen doping step in a way that results in N doped graphene sample with acceptable intensity and $FWHM_{2D}$ the decision were made to apply nitrogen plasma to pristine graphene samples prior to the transfer process.

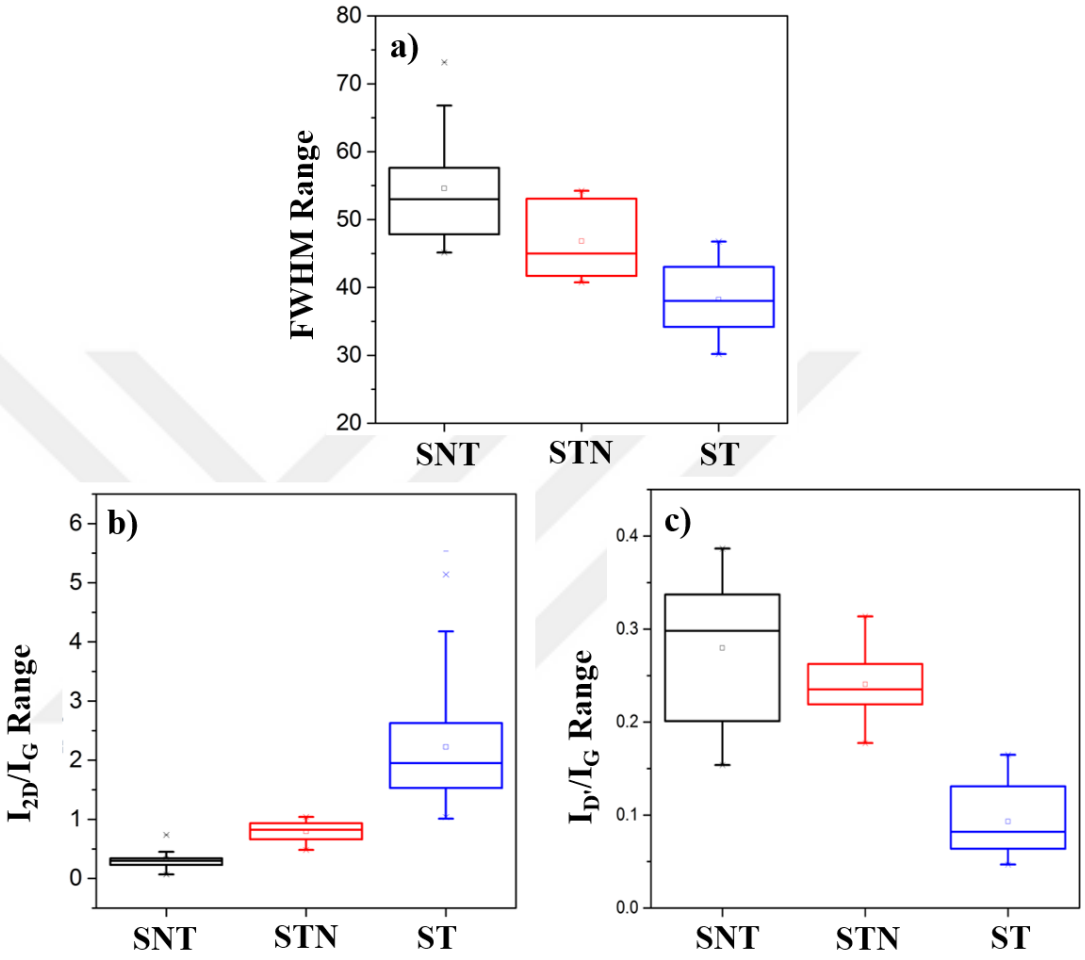

Figure 25 Box charts for a) $FWHM_{2D}$, b) I_{2D}/I_G and c) $I_{D'}/I_G$, of N doped graphene samples prepared before and after transfer as well as pristine graphene on SiO_2/Si.

4.2 N doped Graphene Characterized by Raman

One of the main results obtained from previously reported box charts is that there is no long range order of homogeneity even in a graphene samples with good quality. Figure 26, which is related to Raman spectra of 19 points within 2 parallel lines on a pristine graphene sample, where there was 2mm distance between the points in a line and 5mm distance between the lines, shows the same fact. Although, there is not much difference in number of

layers between different points, there is significant change in the intensity ratio of D band over G band. The non-identical catalytic behavior of different copper planes for methane dehydrogenation and graphene formation as well as grain boundaries, can be the main origin of variation in I_D/I_G. Such heterogeneity in defect density of graphene from point to point, becomes more important during nitrogen doping process, where content of nitrogen atoms and also their configuration in bonding with carbon atoms rely mostly on defects. Consequently, in order to study a large area N doped graphene film with Raman spectroscopy, more spots with less distance from each other had to be characterized.

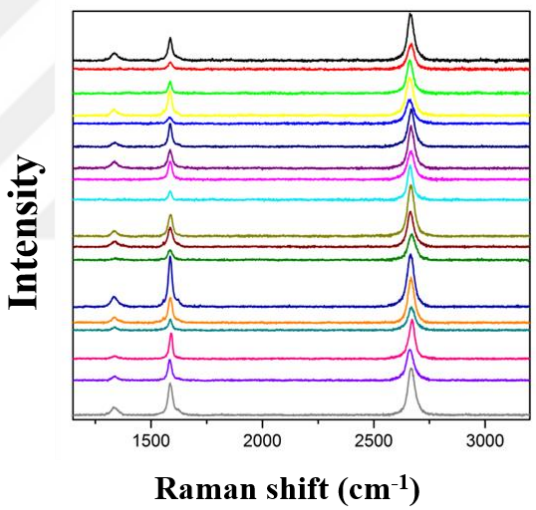

Figure 26 Raman spectra of 19 different points within 2 parallel lines on a pristine graphene sample. There is 2mm distance between each points and 5mm distance between the lines.

Figure 27 demonstrate I_{2D}/I_G (a-b) and I_D/I_G (c-d) Raman maps over an area of 40x40 μm^2 for both pristine and N doped graphene on SiO_2/Si substrate. The resolution of these maps is 0.5 μm. Beside the increase in I_D/I_G, which was previously explained, it is obvious that I_{2D}/I_G has decreased all over the surface. While, intensity ratio of 2D band over G band is normally used to quantify number of layers in graphene, it has also approved that introducing defects to the structure of graphene results in lowering the intensity of 2D peak

due to the opening of channels for one-phonon D band processes, thus decreasing the probability for two-phonon (2D) processes [73]. Presence of dark spots on the I_{2D}/I_G map can be attributed to small graphene flakes on the initial layer of it. Mostly homogenous reddish areas for N doped graphene maps assured us that nitrogen has doped all over the graphene. However, there were 2 issues about these maps which needed to be considered so that one can refer to them as a general condition of graphene after doping nitrogen. First, in order to use N doped graphene in electrochemical applications, a much bigger graphene film than the one showed in Figure 27 (1600 μm^2) was needed, so it was crucial to make sure that the same homogeneity is dominant in other parts of N doped graphene film. Due to the technical limitations, it was impossible to take Raman map from an area in mm scale. Consequently, other maps from different N doped samples (prepared with the same parameters) were taken so that both reproducibility and homogeneity of doping process could be investigated. The results showed same changes in I_{2D}/I_G and I_D/I_G for random parts of other samples prepared under the same parameters. Another important issue was that there is not any direct relation between increase in the intensity of D band and content of doped nitrogen in graphene structure. As a result, the reddish parts in Raman map of N doped graphene could be due to the defects introduce to the graphene because of subjecting it to the harsh plasma environment. The best solution for this problem was to analyze the samples with other characterization techniques and correlate those results with Raman maps. XPS is usually chosen to have a deeper investigation on content and configuration of doped nitrogen atoms.

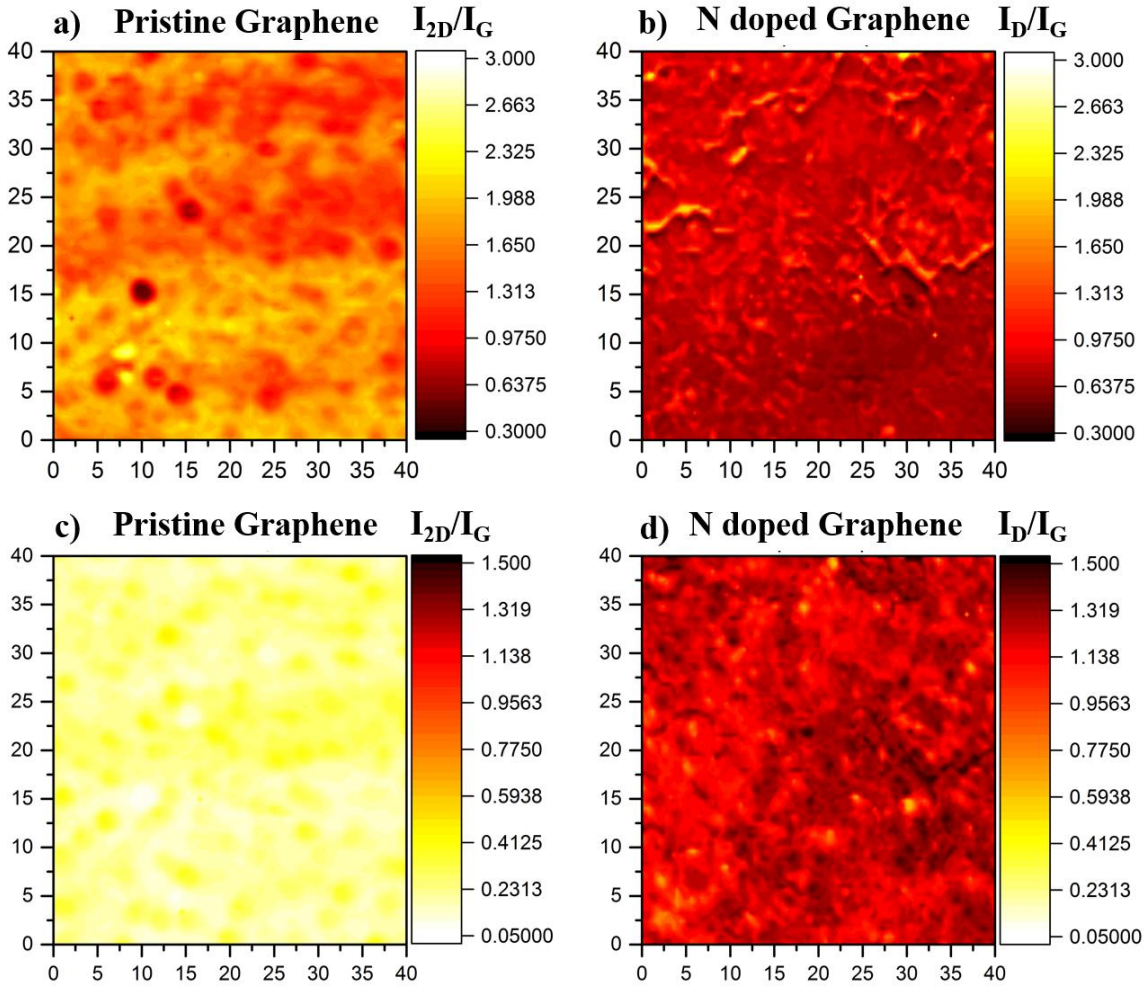

Figure 27 Raman maps for I_{2D}/I_G of a) pristine and b) N doped graphene and Raman maps for I_D/I_G of c) pristine and d) N doped graphene on SiO_2/Si substrate.

Cancado et al. have shown that using I_D/I_G and Equation 8, the average distance between defects (L_D) can be measured [94]. Such quantity is an effective measurement of the amount of disorder in pristine graphene as well as amount of doped nitrogen in the final samples.

$$L_D(nm)^2 = (1.8 \pm 0.5) \times 10^{-2} \times {\lambda_L}^4 (\frac{I_D}{I_G})^{-1} \quad \text{Equation 8}$$

λ_L in above mentioned equation stands for the excitation laser wavelength. According to data obtained from Raman maps, the average I_D/I_G for pristine and N doped graphene were 0.2256 and 1.2150, respectively. As a result, L_D was roughly estimated to be 25 nm for pristine graphene and 10.5 nm for N doped one. Previous studies have shown that the minimum average distance between the defects to convert crystalline sp^2 structure of graphene to amorphous carbon is ~4 nm [73], [98]. So it can be concluded that N doped graphene samples have synthesized while two dimensional crystalline graphene lattice was kept. Meanwhile, density of defects were calculated as $5.1x10^{10}$ cm^2 and $27.3x10^{10}$ cm^2 for pristine and N doped samples, respectively.

4.3 N doped Graphene Characterized by XPS

In this section, the results obtained from XPS investigations will be discussed. The main goals for characterization of N doped graphene samples with XPS were to determine content and configuration of nitrogen as well as homogeneity of doped elements on different parts of the samples. N doped graphene samples were also heated up to mild temperatures, in order to study possible changes in nitrogen configuration under these conditions. The core level high-resolution C 1s and N 1s XPS spectra of pristine and N doped graphene samples on copper substrate are shown in Figure 28a and Figure 28b, respectively. The intensity of C 1s peak dropped significantly and it became broader after doping nitrogen in the structure of graphene. On the other hand, while there was no distinct nitrogen peak for pristine graphene, it was observed for N doped one. All these changes confirms the presence of nitrogen in graphene lattice.

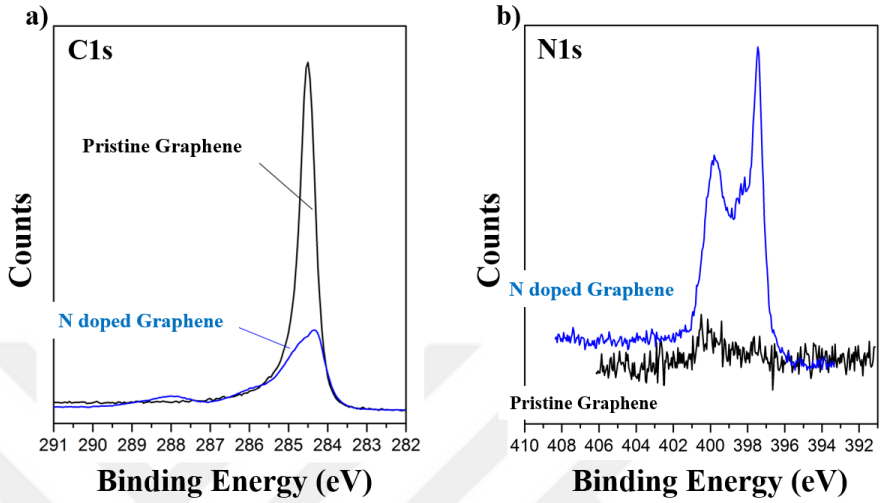

Figure 28 High resolution a) C 1s and b) N 1s ranges for XPS spectra of pristine graphene (black line) and N doped graphene (blue line), obtained by synchrotron generated 700 eV photon.

The C 1s spectrum of pristine graphene was consisted of a single peak centered at 284.5 eV (shown in inset of Figure 29a), which is corresponded to sp^2 carbon [99]. However, the C 1s peak of N doped graphene can be deconvoluted to four individual peaks. Figure 29a shows these peaks, where the ones centered at 284.32 eV and 284.91 eV are assigned to sp^2 carbon and the peak at 285.8 corresponds to N-sp^2 C [15]. The fact that sp^2 carbon peaks were the strongest ones in the N doped sample, indicated that conjugated honeycomb lattice of graphene mostly maintained after doping. According to literatures, there are two main possible bonding assigned for the peak centered at 287.97 eV. the N-sp^3 C peak overlays with C=O at binding energy of 287±0.5 eV [26], [100]. Figure 29b shows that the content of oxygen in the samples has doubled after nitrogen doping. While the initial amount can be attributed to physisorbed oxygen on either sides of graphene, the rest of them increases the possibility of having C=O peak in C 1s spectrum. In addition, investigation on the Cu 3p XPS spectrum (Figure 29c) revealed that oxidation state of copper substrate didn't changed

during nitrogen doping and it remained as metallic Cu. The peaks centered at 75.15 eV and 77.25 correspond to Cu $3p_{3/2}$ and Cu $3p_{1/2}$, respectively [101]. However, due to the long mean free path of 3p electrons of copper, most of the electrons reaching to the detector were coming from the bulk of copper substrate. Consequently, more number of electrons with characteristic energy of metallic copper would reach the detector, making it difficult to identify oxidation state of Cu in its interface with graphene. As a result, Cu 3p spectrum cannot help us in recognizing whether copper had oxidized or not.

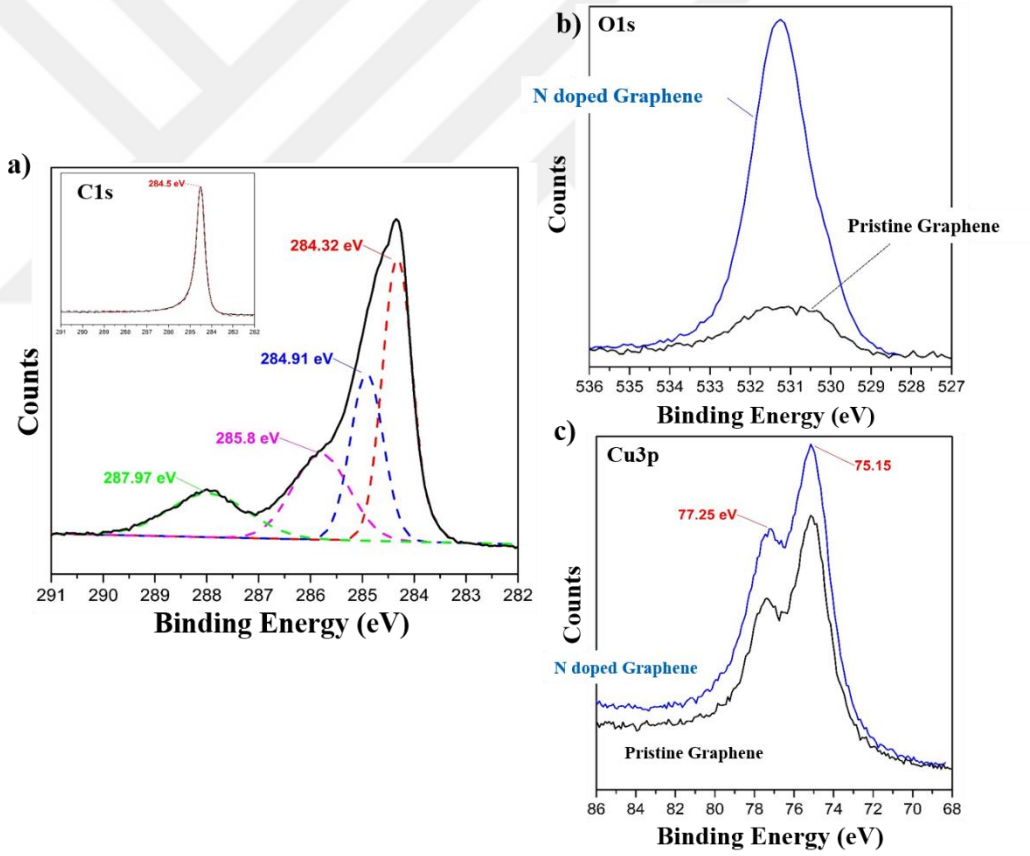

Figure 29 High resolution a) C 1s spectrum of nitrogen doped graphene on copper substrate, deconvoluted to four peaks (the inset is C 1s spectrum for pristine graphene), b) O 1s spectra and c) Cu 3p spectra of pristine and N doped graphene on Cu substrate, obtained by synchrotron generated 700 eV photon.

Deconvolution of O 1s spectrum of N doped graphene revealed that it consists of two peaks (Figure 30). The high bonding energy side peak (531.27 eV), which centered in the same position as O 1s peak of pristine graphene, is usually assigned to C=O bond, while the other one (centered at 529.94 eV) is due to the Cu_2O formation. However our previous experiments showed that even in a N doped graphene sample with significant amount of nitrate groups, approved by N 1s spectrum, it is not possible to distinguish bonds of oxygen to nitrogen from its bonds to carbon by studying O 1s spectrum. As a result, around 3.5% of total oxygen presented in the sample after nitrogen doping was connected to copper and the rest either adsorbed on graphene or bonded to nitrogen. Combination of above mentioned results with quantitative XPS analysis revealed the presence of around 38% nitrogen in graphene structure.

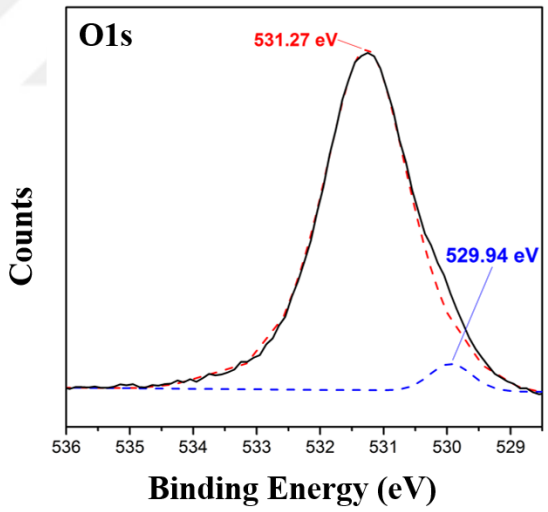

Figure 30 High resolution deconvoluted O 1s spectrum of N doped graphene showing the presence of two peaks at 531.27 and 529.94 eV, obtained by synchrotron generated 700 eV photon.

Due to the notable variety in electrochemical activity of different nitrogen configurations, it is essential to detect type of N-C bonding in graphene. Figure 31 shows that N 1s XPS

spectrum of N doped graphene sample can be fitted by 3 distinct peaks. The most intense peak which is centered at 397.45 eV is assigned to pyridinic nitrogen, while pyrrolic and graphitic nitrogen atoms are shown by the peaks at 398.35 eV and 399.78 eV, respectively. Analysis which was done on the area under the curve of this spectrum revealed that 43% of N atoms doped in graphene was graphitic, while the other two types of configuration (pyridinic and pyrrolic) had almost the same share with concentration of ~28%.

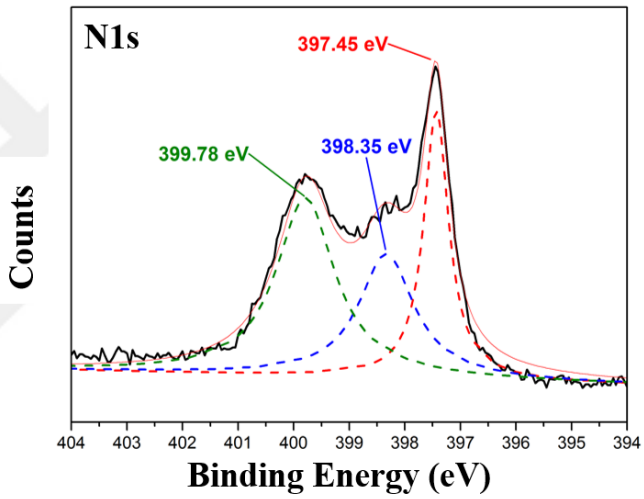

Figure 31 High resolution deconvoluted N 1s spectrum of N doped graphene with three peaks assigned to pyridinic, pyrrolic and graphitic nitrogen, respectively from low binding energy to high bonding energy, obtained by synchrotron generated 700 eV photon.

After making sure about content of each type of nitrogen in the samples, it was important to study the homogeneity of distribution for them in different parts of graphene. Figure 32 shows C 1s (Figure 32a) and N 1s (Figure 32b) spectra taken from three spots on a same sample with 1 mm distance between each spot. As it can be seen, there isn't any significant variation in neither carbon nor nitrogen states in different parts of the sample. This observation is in agreement with homogenous Raman maps that we obtained.

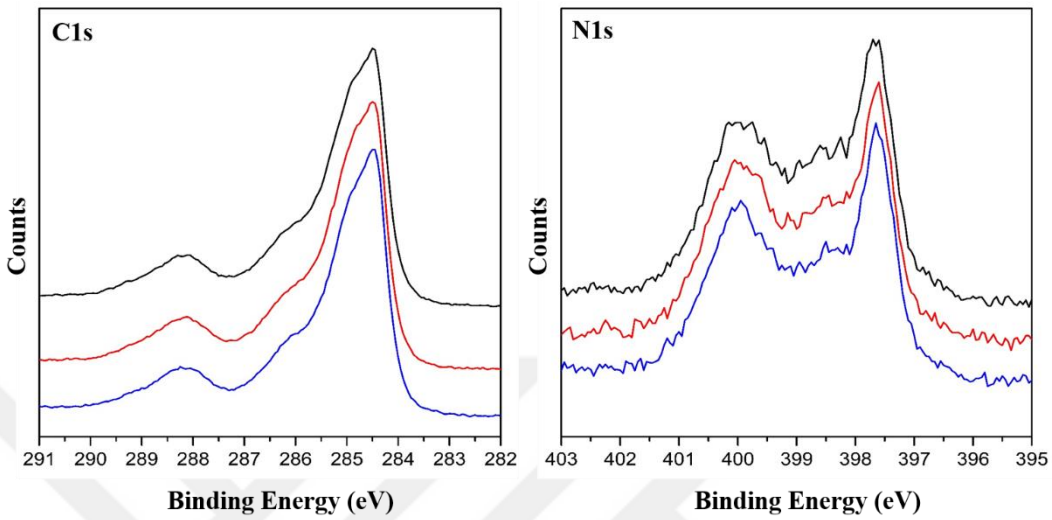

Figure 32 High resolution XPS spectra for a) C 1s and b) N 1s binding energy ranges obtained from three different sports with 1mm distance on N doped graphene sample which was on copper substrate, using synchrotron generated 700 eV photon.

Due to the various operation condition of fuel cells, it is essential to make sure about the properties of N doped graphene at those circumstances. On the other side, different research groups have reported divergent doping percentages by applying almost the same synthesis methods based on CVD. This variation is due to the dependence of the properties of sample to different parameters in both CVD and Plasma techniques, which makes it very difficult to have full control on the features of the final synthesized sample. As a result, finding suitable post treatments, which can control the type and content of nitrogen, would have significant impact on large scale synthesis of nitrogen doped graphene. Heating the samples up to a moderate temperature can be one of these post treatments.

Figure 33 exhibits C 1s (Figure 33a), N 1s (Figure 33b) and O 1s (Figure 33c) XPS spectra of N doped graphene samples. Black spectrum in each of the ranges is related to the sample at room temperature while red and blue ones are associated to the sample at 100 and 150 ^{o}C, respectively. The main changes in Figure 33a are decrease in the intensity of peaks centered

at 285.8 and 287.97 eV. The significant decrease of the area under the curve of first peak cannot give a comprehensive result by itself, since it can be attributed to either pyridinic or graphitic doped nitrogen. There is a similar situation for the peak at 287.97 as well, because both C=O and N-sp^3 C bonding have contributions in it. However, N 1s spectrum (Figure 33b) revealed that the main effect of increasing temperature was to break the bonds between carbon and graphitic nitrogen. Also according the Figure 33c, copper has oxidized more by increasing the temperature. The oxygen needed for this oxidization can be supplied by either the adsorbed oxygen between graphene and copper or by breaking C=O bonds. The second scenario seems more probable, since the high bonding energy peak of C 1s spectrum has dropped but there is still a significant peak for pyrrolic nitrogen. So the remaining peak at 287.97 eV for the N doped graphene at 150 ^{o}C is mainly assigned to nitrogen groups. Quantitative XPS analysis revealed that content of nitrogen has not changed in interval of 25-150 ^{o}C.

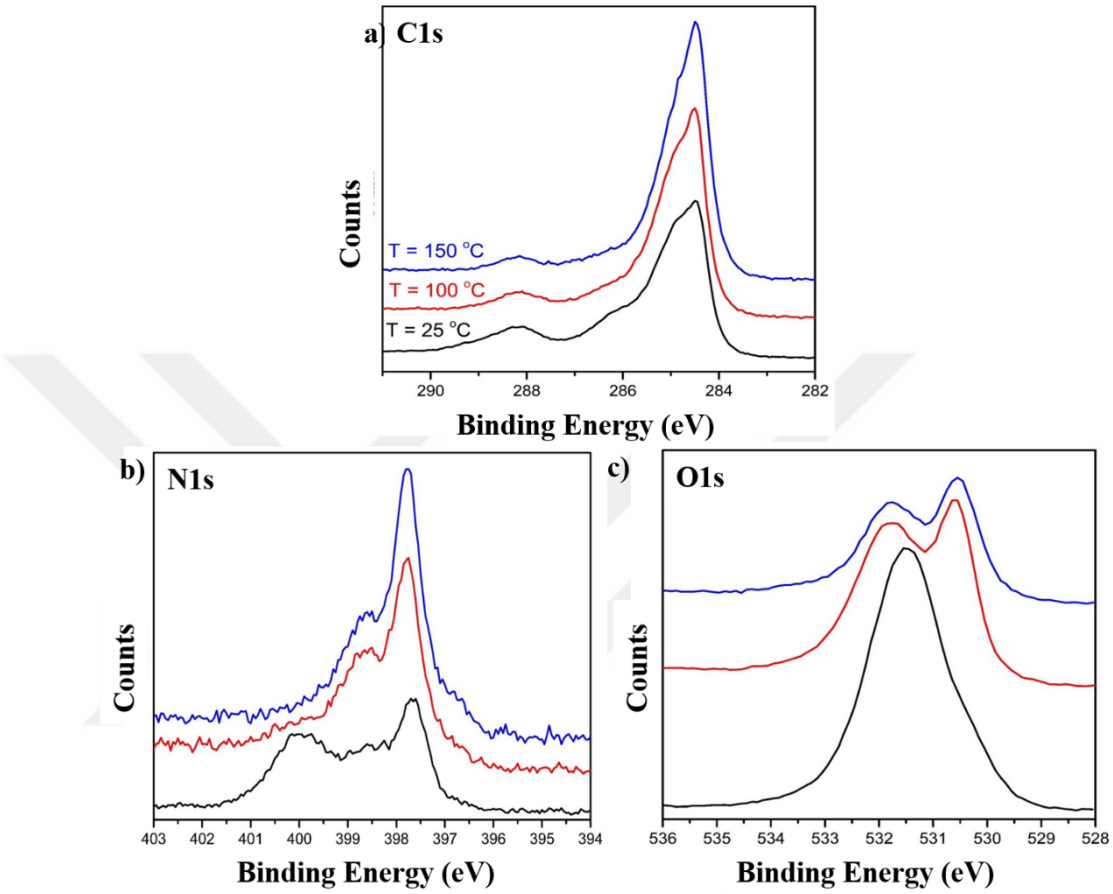

Figure 33 High resolution spectrum of a) C 1s, b) N 1s and c) O 1s for N doped graphene sample at different temperatures, obtained by synchrotron generated 700 eV photon. The black, blue and red lines are assigned to 25, 100 and 150 ºC, respectively.

Above mentioned results showed that nitrogen atoms tend to choose pyridinic and pyrrolic configurations if necessary amount of energy is supplied to them (by heating). So if these configurations are more favorable, they would be the first priorities for nitrogen atoms to bond to carbon lattice. In order to investigate the probability of this hypothesis, N doped sample with low concentration of graphene (~6.5%) was prepared using N_2 plasma. Figure

34 shows N 1s high resolution XPS spectrum of this sample. As it can be seen, while characteristic peaks for pyridinic and pyrrolic nitrogen atoms are present at binding energy of 398.5 eV and 399.8 eV, respectively, no graphitic nitrogen exists in graphene structure. Consequently, it seems that nitrogen atoms have selectivity in their configuration up to a certain concentration. However, by further increasing nitrogen coverage they start to attach to carbon atoms randomly and take graphitic configuration as well. There might be the same procedure for nitrogen atoms to choose between pyridinic and pyrrolic sites in lower concentrations.

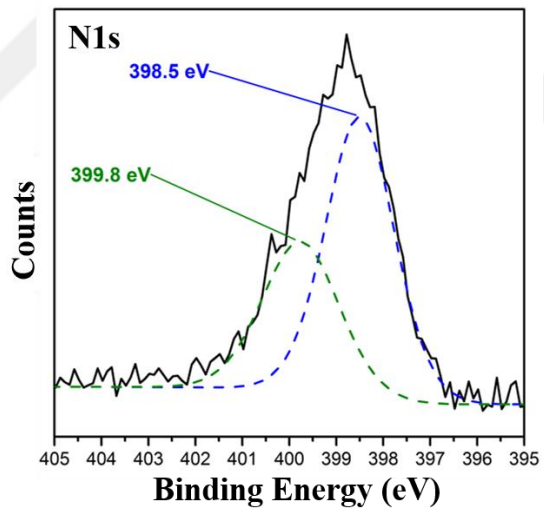

Figure 34 High resolution deconvoluted N 1s spectrum of N doped graphene with low nitrogen concentration showing two peaks assigned to pyridinic and pyrrolic nitrogen, respectively from low binding energy to high bonding energy.

The effect of heat treatment on the N doped samples with low coverage was investigated by treating them in 100 ^{o}C, 200 ^{o}C, 300 ^{o}C and 400 ^{o}C for 5 minutes. The atmosphere of CVD system was filled with Ar and the pressure was ~0.5 Torr. Figure 35 depicts C 1s

(Figure 35a), N 1s (Figure 35b) and O 1s (Figure 35c) XPS spectra of these samples. The Black spectrum in each of the ranges is related to the sample at room temperature while the heat treated samples are shown with unique colors which are the same among all three figures. It can be seen that while sp^2 carbon peak at C 1s spectrum is not changed during heat treatment, the small peak at high binding energy side is removed after reaching to 200 ^oC. As discussed before, this peak can be assigned to either C=O or N-S sp^3 groups (pyridinic and pyrrolic nitrogen atoms). Area under the peak analysis of N 1s spectra revealed that the concentration of nitrogen atoms bonded to carbon lattice was constant up to 200 ^oC, but further increasing the temperature resulted in loosing almost one percent for every 100 ^oC. As a result, the sharp drop of the peak at binding energy of ~288 eV in C 1s spectrum is not due to the any break in the bonds between nitrogen and carbon atoms. Consequently, this peak is attributed to C=O groups which are broken in temperatures above 200 ^oC. Such trend in breaking of C=O bonds is in agreement with our previous results for N doped samples with high concentration of oxygen. It is also obvious that nitrate groups (confirmed by the peak at binding energy of ~406.5 eV of N 1s spectrum) are removed after reaching to 200 ^oC. However, there is not any significant configuration change in nitrogen atoms even at 400 ^oC. Figure 35c revealed that copper is oxidized by increasing the temperature, but it seems that most of oxygen atoms have left the sample at 400 ^oC. The origin of oxygen atoms for copper to be oxidized is the same as previous samples with high concentration of nitrogen, where trapped oxygen between graphene and Cu was introduced as the main source.

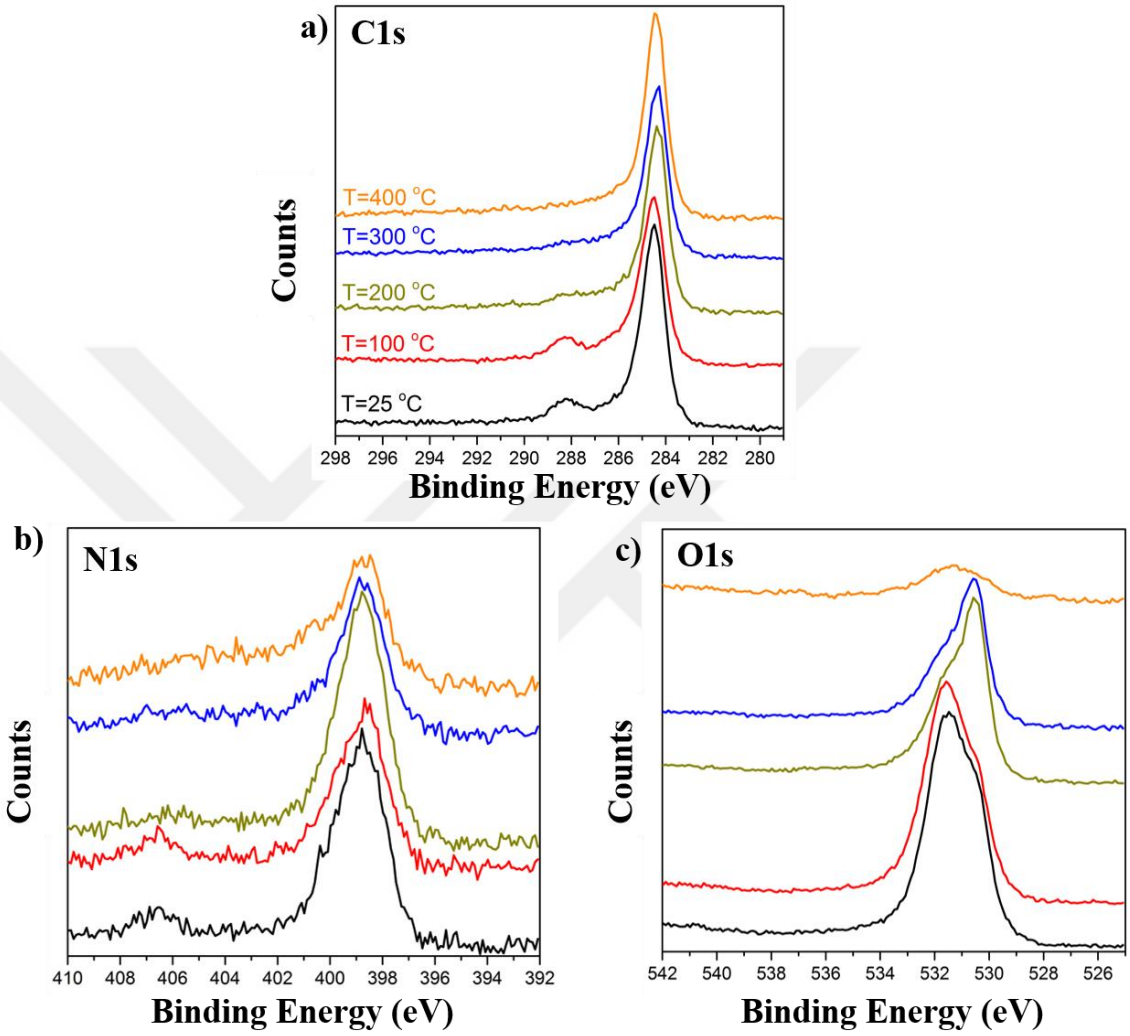

Figure 35 High resolution spectrum of a) C 1s, b) N 1s and c) O 1s for N doped graphene sample with low nitrogen concentration at different temperatures. The black, red, dark yellow, blue and orange lines are assigned to 25, 100, 200, 300 and 400 ºC, respectively.

4.4 N doped Graphene Characterized by AFM

AFM has been used in some of the studies for characterization of graphene in order to determine number of layers [102]. In this study, AFM was carried out to investigate both number of layers and the change in topography of graphene after doping nitrogen into its structure. Schniepp et al, have shown that the height of a single layer graphene sheet is about 0.8 nm [103], however in majority of the parts of the pristine and N doped graphene samples characterized by AFM, the height is about 1 nm. The origin of this slight difference can be oxygen atoms adsorbed on both sides of graphene [104]. Figure 36 shows AFM images for pristine (Figure 36a) and N doped graphene (Figure 36b) as well as their line profiles. The main effect of nitrogen plasma observable in AFM, was to eliminate small graphene islands (shown with green arrow in Figure 36a) and carbon nanoparticles from surface of main graphene sheet. However there were some nanoparticles remaining on the surface which could be due to the low plasma apply duration (Nitrogen plasma was applied to graphene samples for 5 minutes). Presence of the islands is in agreement with appearance of dark spots in I_{2D}/I_G Raman map. Since there are more number of layers in these points, the I_{2D}/I_G was decreased. On the other hand these islands cannot be attributed to any material rather than graphene because no spot without 2D peak was observed in Raman map characterization. Line profile of N doped graphene revealed that synthesized samples were mainly consisted of 1-2 layers of graphene.

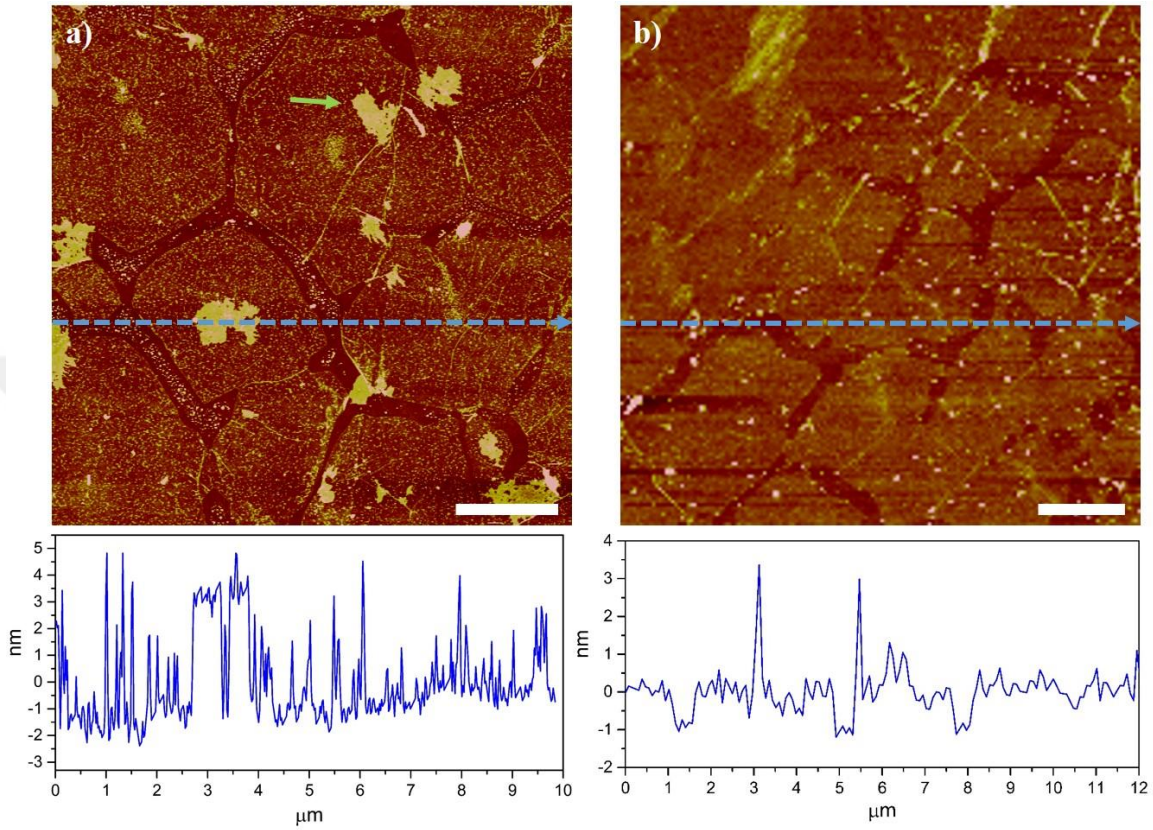

Figure 36 AFM images and corresponded height profile of a) pristine and b) N doped graphene samples transferred on SiO_2/Si substrate. The blue horizontal dashed line shows the related profile position. White scale bar in left bottom corner of images is 2µm.

Chapter 5
Conclusion and Future Works

In this study, graphene films were synthesized by chemical vapor deposition method by modified growth parameters (methane flow rate, synthesis temperature, growth time, heating rate and total pressure of the system). It was observed that heating 25 μm thick multi-crystalline copper foil to 950 ^{o}C in presence of argon and exposing the foil to hydrogen were two crucial factors prior to the main synthesis step. Clean surface with less roughness and larger flat grains provides surface needed for synthesis of few layer graphene with high crystallinity. It was also found that growth kinetics were strongly influenced by total pressure, methane partial pressure, and exposure time.

Nitrogen atoms were doped into the graphene structure by exposing the pristine graphene samples to N_2 plasma environment. Correlated results obtained by Raman spectroscopy, XPS and AFM revealed that homogeneous N doped graphene samples with ~38% concentration of N atoms were synthesized. 43% of these nitrogen atoms were attached to carbon lattice with graphitic configuration and the rest of them were almost equally divided to pyridinic and pyrrolic nitrogen groups.

Mild heat treatment of N doped graphene samples with high concentration of nitrogen caused conversion of graphitic nitrogen atoms to pyridinic and pyrrolic nitrogen while total concentration of the nitrogen was the same as untreated samples. Preparing N doped graphene samples with lower concentration of nitrogen (~6%) revealed that these samples consist of only pyridinic and pyrrolic groups which do not show any change in nitrogen configuration even if the samples are heated up to 400 ^{o}C.

According to the results obtained in this study, below mentioned tasks are suggested in order to have a more comprehensive study on synthesis and characterization of N doped graphene:

- Synthesis of pristine graphene using 5 sccm of methane.
- Synthesis of N doped graphene samples using different plasma power, plasma exposure time and temperature.
- XPS characterization of the N doped graphene samples exposed to nitrogen plasma before and after transfer.
- Synthesis of N doped graphene sample by doping nitrogen both before and after transfer and characterize it with Raman spectroscopy and XPS.
- Investigation on N doped graphene samples with very low concentration of nitrogen in order to find possible critical point where nitrogen choose only one configuration.
- Investigation on N doped graphene samples in order to clarify the highest possible nitrogen doping with only pyridinic and pyrrolic groups without any post synthesis treatments.

Chapter 6
References

[1] M. J. Allen, V. C. Tung, and R. B. Kaner, "Honeycomb Carbon : A Review of Graphene," *Chem. Rev.*, vol. 110, no. 1, pp. 132–145, 2010.

[2] D. J. K. S. Novoselov, A. K. Geim, S. V. Morozov and A. A. F. Y. Zhang, S. V. Dubonos, I. V. Grigorieva, "Electric Field Effect in Atomically Thin Carbon Films," *Science (80-.).*, 2004.

[3] C. N. R. Rao, A. K. Sood, K. S. Subrahmanyam, and A. Govindaraj, "Graphene : The New Two-Dimensional Nanomaterial," *Angew. Chemie Int. Ed.*, vol. 48, pp. 7752–7777, 2009.

[4] J. Hicks, K. Shepperd, and F. Wang, "The growth and morphology of epitaxial multilayer graphene," *IOP Sci.*, vol. 20, no. 1, 2008.

[5] W. Choi and Y. S. et al. Kang, "Synthesis of Graphene and Its Applications : A Review," *Crit. Rev. Solid State Mater. Sci.*, vol. 35, no. 1, pp. 52–71, 2010.

[6] K. S. A. Novoselov, A. K. Geim, Sv. Morozov, D. Jiang, Mi. Katsnelson, Iv. Grigorieva, Sv. Dubonos, and Aa. Firsov, "Two-dimensional gas of massless Dirac fermions in graphene," *Nature*, vol. 438, no. 7065, pp. 197–200, 2005.

[7] K. A. Ritter and J. W. Lyding, "The influence of edge structure on the electronic properties of graphene quantum dots and nanoribbons," *Nat. Mater.*, vol. 8, no. 3, pp. 235–242, 2009.

[8] F. Schedin, A. K. Geim, S. V Morozov, E. W. Hill, P. Blake, M. I. Katsnelson, and K. S. Novoselov, "Detection of individual gas molecules adsorbed on graphene," *Nat. Mater.*, vol. 6, no. 9, pp. 652–655, 2007.

[9] W. Chen and S. et al. Wee, "Surface Transfer p-Type Doping of Epitaxial Graphene," *J. Am. Chem. Soc.*, vol. 129, no. 16, pp. 10418–10422, 2007.

[10] G. Giovannetti, P. A. Khomyakov, G. Brocks, V. M. Karpan, J. Van Den Brink, and P. J. Kelly, "Doping Graphene with Metal Contacts," *Phys. Rev. Lett.*, vol. 26803, no. July, pp. 4–7, 2008.

[11] Wang, Xinran, Li, Xiaolin, and H. et al. Dai, "N-Doping of Graphene Through Electrochemical Reactions with Ammonia," *Science (80-.).*, vol. 8, no. May, pp. 768–771, 2009.

[12] Y. Shao, S. Zhang, M. H. Engelhard, G. Li, G. Shao, Y. Wang, J. Liu, I. A. Aksay, and Y. Lin, "Nitrogen-doped graphene and its electrochemical applications," *J. Mater. Chem.*, no. 20, pp. 7491–7496, 2010.

[13] Z. Luo and J. et al. Lin, "Pyridinic N doped graphene: synthesis, electronic structure, and electrocatalytic property," *J. Mater. Chem.*, vol. 21, pp. 8038–8044, 2011.

[14] H. Gao, L. Song, W. Guo, L. Huang, D. Yang, F. Wang, Y. Zuo, X. Fan, Z. Liu, W. Gao, R. Vajtai, K. Hackenberg, and P. M. Ajayan, "A simple method to synthesize continuous large area nitrogen-doped graphene," *Carbon N. Y.*, vol. 50, no. 12, pp. 4476–4482, 2012.

[15] D. Wei, Y. Liu, Y. Wang, H. Zhang, L. Huang, and G. Yu, "Synthesis of N-Doped Graphene by Chemical Vapor Deposition and Its Electrical Properties," *Nano Lett.*, vol. 9, no. 5, pp. 1752–1758, 2009.

[16] X. Dong, P. Wang, W. Fang, C.-Y. Su, Y.-H. Chen, L.-J. Li, W. Huang, and P. Chen, "Growth of large-sized graphene thin-films by liquid precursor-based chemical vapor deposition under atmospheric pressure," *Carbon N. Y.*, vol. 49, no. 11, pp. 3672–3678, 2011.

[17] C. Zhang, L. Fu, N. Liu, M. Liu, Y. Wang, and Z. Liu, "Synthesis of Nitrogen-Doped Graphene Using Embedded Carbon and Nitrogen Sources," *Adv. Mater.*, vol. 23, pp. 1020–1024, 2011.

[18] D. Deng, X. Pan, L. Yu, Y. Cui, Y. Jiang, J. Qi, W. Li, Q. Fu, X. Ma, Q. Xue, G. Sun,

and X. Bao, “Toward N-Doped Graphene via Solvothermal Synthesis,” *Chem. Mater.*, vol. 23, pp. 1188–1193, 2011.

[19] B. Guo, Q. Liu, E. Chen, H. Zhu, L. Fang, and J. R. Gong, “Controllable N-Doping of Graphene,” *Nano Lett.*, vol. 10, pp. 4975–4980, 2010.

[20] D. Geng, “High oxygen-reduction activity and durability of nitrogen-doped graphene,” *Energy Environ. Sci.*, no. 4, pp. 760–764, 2011.

[21] D. Long, W. Li, L. Ling, J. Miyawaki, I. Mochida, and S. Yoon, “Preparation of Nitrogen-Doped Graphene Sheets by a Combined Chemical and Hydrothermal Reduction of Graphene Oxide,” *Langmuir*, vol. 26, no. 24, pp. 16096–16102, 2010.

[22] R. I. Jafri, N. Rajalakshmi, and S. Ramaprabhu, “Nitrogen doped graphene nanoplatelets as catalyst support for oxygen reduction reaction in proton exchange membrane fuel cell,” *J. Mater. Chem.*, vol. 20, pp. 7114–7117, 2010.

[23] H. M. Jeong, J. W. Lee, W. H. Shin, Y. J. Choi, H. J. Shin, J. K. Kang, and J. W. Choi, “Nitrogen-Doped Graphene for High-Performance Ultracapacitors and the Importance of Nitrogen-Doped Sites at Basal Planes,” *Nano Lett.*, vol. 11, pp. 2472–2477, 2011.

[24] Y.-C. Lin, C.-Y. Lin, and P.-W. Chiu, “Controllable graphene N-doping with ammonia plasma,” *Appl. Phys. Lett.*, vol. 96, no. 13, p. 133110, 2010.

[25] H. Wang, T. Maiyalagan, and X. Wang, “Review on Recent Progress in Nitrogen-Doped Graphene : Synthesis , Characterization , and Its Potential Applications,” *ACS Catal.*, vol. 2, pp. 781–794, 2012.

[26] Y. Wang, Y. Shao, D. W. Matson, J. Li, and Y. Lin, “Nitrogen-Doped Graphene and Its Biosensing,” *ACS Nano*, vol. 4, no. 4, pp. 1790–1798, 2010.

[27] Y. Yu, Y. Hu, X. Liu, W. Deng, and X. Wang, “Electrochimica Acta The study of Pt@Au electrocatalyst based on Cu underpotential deposition and Pt redox replacement,” *Electrochem. Acta*, vol. 54, pp. 3092–3097, 2009.

[28] M. Neergat, A. K. Shukla, K. S. Gandhi, S. State, and S. C. Unit, "Platinum-based alloys as oxygen ± reduction catalysts for solid ± polymer ± electrolyte direct methanol fuel cells," *J. Appl. Electrochem.*, vol. 31, pp. 373–378, 2001.

[29] M. Winter and J. R. Brodd, "What Are Batteries , Fuel Cells , and Supercapacitors ?," *Chem. Rev.*, vol. 104, no. 10, pp. 4245–4269, 2004.

[30] B. et al. Winther-Jensen, "High Rates of Oxygen Reduction," *Science (80-.).*, vol. 321, no. August, pp. 671–674, 2008.

[31] J. P. Collman, N. K. Devaraj, R. A. Decréau, Y. Yang, Y. Yan, W. Ebina, T. A. Eberspacher, and C. E. D. Chidsey, "A Cytochrome c Oxidase Model Under Rate-Limiting Electron Flux," *Science (80-.).*, vol. 315, pp. 1565–1569, 2007.

[32] K. Gong, P. Yu, L. Su, S. Xiong, and L. Mao, "Polymer-Assisted Synthesis of Manganese Dioxide/Carbon Nanotube Nanocomposite with Excellent Electrocatalytic Activity toward Reduction of Oxygen," *J. Phys. Chem. C*, vol. 111, pp. 1882–1887, 2007.

[33] B. C. H. Steele and A. Heinzel, "Materials for fuel-cell technologies," *Nature*, vol. 414, no. November, pp. 345–352, 2001.

[34] L. Zhang and Z. Xia, "Mechanisms of Oxygen Reduction Reaction on Nitrogen-Doped Graphene for Fuel Cells," *J. Phys. Chem. C*, vol. 115, pp. 11170–11176, 2011.

[35] Z. Sheng, L. Shao, J. Chen, W. Bao, F. Wang, and X. Xia, "Catalyst-Free Synthesis of Nitrogen- Doped Graphene via Thermal Annealing Graphite Oxide with Melamine and Its Excellent Electrocatalysis," *ACS Nano*, vol. 5, no. 6, pp. 4350–4358, 2011.

[36] Z. Luo, "Pyridinic N doped graphene: synthesis, electronic structure, and electrocatalytic property," *J. Mater. Chem.*, pp. 8038–8044, 2011.

[37] U. A. Paulus, T. J. Schmidt, H. A. Gasteiger, and R. J. Behm, "Oxygen Reduction on a High-Surface Area Pt/Vulcan Carbon Catalyst : a Thin-Film Rotating Ring-Disk Electrode Study," *J. Electroanal. Chem.*, vol. 495, pp. 134–145, 2001.

[38] Z. Wu and D. et al. Zhao, “Ordered mesoporous graphitized pyrolytic carbon materials : synthesis , graphitization , and electrochemical properties,” *J. Mater. Chem.*, vol. 22, pp. 8835–8845, 2012.

[39] L. Qu, Y. Liu, J. Baek, and L. D. Ḱ, “Nitrogen-Doped Graphene as Efficient Metal-Free Electrocatalyst for Oxygen Reduction in Fuel Cells,” *ACS Nano*, vol. 4, no. 3, pp. 1321–1326, 2010.

[40] Y. Okamoto, “Applied Surface Science First-Principles Molecular Dynamics Simulation of O2 Reduction on Nitrogen-Doped Carbon,” *Appl. Surf. Sci.*, vol. 256, pp. 335–341, 2009.

[41] L. Zhang, X. Liang, W. Song, and Z. Wu, “Identification of the nitrogen species on N-doped graphene layers and Pt / NG composite catalyst for direct methanol fuel cell,” *Phys. Chem. Chem. Phys.*, vol. 12, pp. 12055–12059, 2010.

[42] M. N. Groves, A. S. W. Chan, C. Malardier-jugroot, and M. Jugroot, “Improving platinum catalyst binding energy to graphene through nitrogen doping,” *Chem. Phys. Lett.*, vol. 481, no. 4–6, pp. 214–219, 2009.

[43] Y. Yao and C. Wong, “Monolayer graphene growth using additional etching process in atmospheric pressure chemical vapor deposition,” *Carbon N. Y.*, vol. 50, no. 14, pp. 5203–5209, 2012.

[44] J. K. Wassei, M. Mecklenburg, J. A. Torres, J. D. Fowler, B. C. Regan, R. B. Kaner, and B. H. Weiller, “Chemical vapor deposition of graphene on copper from methane, ethane and propane: Evidence for bilayer selectivity,” *Small*, vol. 8, no. 9, pp. 1415–1422, 2012.

[45] H. Pedersen and S. D. Elliott, “Studying Chemical Vapor Deposition Processes with Theoretical Chemistry,” *Theor. Chem. Accounts*, pp. 1–10, 2014.

[46] X. Li, C. W. Magnuson, A. Venugopal, R. M. Tromp, J. B. Hannon, E. M. Vogel, L. Colombo, and R. S. Ruoff, “Large-area graphene single crystals grown by low-

pressure chemical vapor deposition of methane on copper," *J. Am. Chem. Soc.*, vol. 133, no. 9, pp. 2816–2819, 2011.

[47] I. Vlassiouk, P. Fulvio, H. Meyer, N. Lavrik, S. Dai, P. Datskos, and S. Smirnov, "Large scale atmospheric pressure chemical vapor deposition of graphene," *Carbon N. Y.*, vol. 54, pp. 58–67, 2013.

[48] Z. Li, P. Wu, C. Wang, X. Fan, W. Zhang, X. Zhai, C. Zeng, Z. Li, J. Yang, and J. Hou, "Low-temperature growth of graphene by chemical vapor deposition using solid and liquid carbon sources," *ACS Nano*, vol. 5, no. 4, pp. 3385–3390, 2011.

[49] R. Addou, A. Dahal, P. Sutter, and M. Batzill, "Monolayer graphene growth on Ni(111) by low temperature chemical vapor deposition," *Appl. Phys. Lett.*, vol. 100, no. 2, pp. 4–7, 2012.

[50] C.-M. Seah, S.-P. Chai, and A. R. Mohamed, "Mechanisms of graphene growth by chemical vapour deposition on transition metals," *Carbon N. Y.*, vol. 70, no. 0, pp. 1–21, 2014.

[51] N. K. Memon, S. D. Tse, M. Chhowalla, and B. H. Kear, "Role of substrate, temperature, and hydrogen on the flame synthesis of graphene films," *Proc. Combust. Inst.*, vol. 34, no. 2, pp. 2163–2170, 2013.

[52] M. Regmi, M. F. Chisholm, and G. Eres, "The effect of growth parameters on the intrinsic properties of large-area single layer graphene grown by chemical vapor deposition on Cu," *Carbon N. Y.*, vol. 50, no. 1, pp. 134–141, 2012.

[53] X. Li, C. W. Magnuson, A. Venugopal, J. An, J. W. Suk, B. Han, M. Borysiak, W. Cai, A. Velamakanni, Y. Zhu, L. Fu, E. M. Vogel, E. Voelkl, L. Colombo, and R. S. Ruoff, "Graphene films with large domain size by a two-step chemical vapor deposition process," *Nano Lett.*, vol. 10, no. 11, pp. 4328–4334, 2010.

[54] M. Losurdo, M. M. Giangregorio, P. Capezzuto, and G. Bruno, "Graphene CVD growth on copper and nickel: role of hydrogen in kinetics and structure," *Phys. Chem.*

Chem. Phys., vol. 13, no. 46, p. 20836, 2011.

[55] I. Vlassiouk, M. Regmi, P. Fulvio, S. Dai, P. Datskos, G. Eres, and S. Smirnov, "Role of hydrogen in chemical vapor deposition growth of large single-crystal graphene," *ACS Nano*, vol. 5, no. 7, pp. 6069–6076, 2011.

[56] Y. Zhang, Z. Li, P. Kim, L. Zhang, and C. Zhou, "Anisotropic hydrogen etching of chemical vapor deposited graphene," *ACS Nano*, vol. 6, no. 1, pp. 126–132, 2012.

[57] G. E. Ivan Vlassiouk, Murari Regmi, Pasquale Fulvio, Sheng Dai, Panos Datskos, "Role of Hydrogen in Chemical Vapor Deposition Growth of Large Single-Crystal Graphene," *ACS Nano*, vol. 5, no. 7, pp. 6069–6076, 2011.

[58] X. Li, W. Cai, J. An, S. Kim, J. Nah, D. Yang, L. Colombo, and R. S. Ruoff, "Large-Area Synthesis of High-Quality and Uniform Graphene Films on Copper Foils," *Science (80-.).*, vol. 3893, no. June, pp. 1312–1315, 2009.

[59] Y. I. Zhang, L. Zhang, and C. Zhou, "Review of Chamical Vapor Deposition of Graphene and Related Applications," *Acc. Chem. Res.*, vol. 46, no. 10, pp. 2329–2339, 2013.

[60] G. H. Han, F. Güneş, J. J. Bae, E. S. Kim, S. J. Chae, H. J. Shin, J. Y. Choi, D. Pribat, and Y. H. Lee, "Influence of copper morphology in forming nucleation seeds for graphene growth," *Nano Lett.*, vol. 11, no. 10, pp. 4144–4148, 2011.

[61] A. Grill, *Cold plasma in materials fabrication*, vol. 151. IEEE Press, New York, 1994.

[62] D. A. Gurnett and A. Bhattacharjee, "Introduction to Plasma Physiscs; With Space and Laboratory Applications," 2005.

[63] H. Conards and Schmidt M, "Plasma generation and plasma sources," *IOP Sci.*, vol. 9, pp. 441–454, 2000.

[64] K. Iwaszczuk, M. Zalkovskij, A. C. Strikwerda, and P. U. Jepsen, "Nitrogen plasma formation through terahertz-induced ultrafast electron field emission," *Optica*, vol. 2, no. 2, p. 116, 2015.

[65] S. Mazouffre, C. Foissac, P. Supiot, P. Vankan, R. Engeln, D. C. Schram, and N. Sadeghi, "Density and temperature of N atoms in the afterglow of a microwave discharge measured by a two-photon laser-induced fluorescence technique," *Plasma Sources Sci. Technol*, vol. 10, pp. 168–175, 2001.

[66] Y. Kubota, R. Ichiki, T. Hara, N. Yamaguchi, and Y. Takemura, "Spectroscopic analysis of nitrogen atmospheric plasma jet," *J. Plasma Fusion Res*, vol. 8, pp. 740–743, 2009.

[67] S. Goniszewski, J. Gallop, M. Adabi, K. Gajewski, O. Shaforost, N. Klein, A. Sierakowski, J. Chen, Y. Chen, and T. Gotszalk, "Self-supporting graphene films and their applications," *IET Circuits, Devices Syst.*, vol. 9, no. 6, pp. 420–427, 2015.

[68] X. Liang, B. A. Sperling, I. Calizo, G. Cheng, C. A. Hacker, Q. Zhang, Y. Obeng, K. Yan, H. Peng, and Q. Li, "Toward clean and crackless transfer of graphene," *ACS Nano*, vol. 5, no. 11, pp. 9144–9153, 2011.

[69] R. Haynes, *Optical Microscopy of Materials*. Springer US, 2013.

[70] Y. H. Zhang, B. Wang, H. R. Zhang, Z. Y. Chen, Y. Q. Zhang, B. Wang, Y. P. Sui, X. L. Li, X. M. Xie, G. H. Yu, Z. Jin, and X. Y. Liu, "The distribution of wrinkles and their effects on the oxidation resistance of chemical vapor deposition graphene," *Carbon N. Y.*, vol. 70, pp. 81–86, 2014.

[71] R. P. Vidano, D. B. Fischbach, L. J. Willis, and T. M. Loehr, "Observation of Raman band shifting with excitation wavelength for carbons and graphites," *Solid State Commun.*, vol. 39, no. 2, pp. 341–344, 1981.

[72] F. Tuinstra and L. Koenig, "Raman Spectrum of Graphite," *J. Chem. Phys.*, vol. 53, no. 1970, pp. 1126–1130, 1970.

[73] A. Jorio and M. et al. Lucchese, "Raman study of ion-induced defects in N -layer graphene," *J. Phys. Condens. Matter*, vol. 22, 2010.

[74] C. Thomsen and S. Reich, "Double resonant Raman scattering in graphite," *Phys. Rev.*

Lett., vol. 85, no. 24, p. 5214, 2000.

[75] R. Saito, A. Jorio, A. G. Souza Filho, G. Dresselhaus, M. S. Dresselhaus, and M. A. Pimenta, "Probing phonon dispersion relations of graphite by double resonance Raman scattering," *Phys. Rev. Lett.*, vol. 88, no. 2, p. 27401, 2001.

[76] R. Saito, M. Hofmann, G. Dresselhaus, A. Jorio, M. S. Dresselhaus, M. Hofmann, G. Dresselhaus, A. Jorio, and M. S. Dresselhaus, "Raman Spectroscopy of Graphene and Carbon Nanotubes," *Adv. Phys.*, vol. 8732, no. November, pp. 413–550, 2016.

[77] M.M. Lucchese, R. B. Capaz, C. A. Achete, and A. Jorio, "Quantifying ion-induced defects and Raman relaxation length in graphene," *Carbon N. Y.*, vol. 48, no. 5, pp. 1592–1597, 2010.

[78] A. C. Ferrari, "Raman spectroscopy of graphene and graphite: Disorder, electron-phonon coupling, doping and nonadiabatic effects," *Solid State Commun.*, vol. 143, no. 1–2, pp. 47–57, 2007.

[79] D. M. Basko, S. Piscanec, and A. C. Ferrari, "Electron-electron interactions and doping dependence of the two-phonon Raman intensity in graphene," *Phys. Rev. B*, vol. 80, no. 16, p. 165413, 2009.

[80] C. Casiraghi, S. Pisana, K. S. Novoselov, A. K. Geim, and A. C. Ferrari, "Raman fingerprint of charged impurities in graphene," *Appl. Phys. Lett.*, vol. 91, no. 23, p. 233108, 2007.

[81] E. H. M. Ferreira, M. V. O. Moutinho, F. Stavale, M. M. Lucchese, R. B. Capaz, C. A. Achete, and A. Jorio, "Evolution of the Raman spectra from single-, few-, and many-layer graphene with increasing disorder," *Phys. Rev. B*, vol. 82, no. 12, p. 125429, 2010.

[82] A. C. Ferrari, J. C. Meyer, V. Scardaci, C. Casiraghi, M. Lazzeri, F. Mauri, S. Piscanec, D. Jiang, K. S. Novoselov, S. Roth, and A. K. Geim, "Raman Spectrum of Graphene and Graphene Layers," *Phys. Rev.*, vol. 187401, no. NOVEMBER, pp. 1–

4, 2006.

[83] P. Van Der Heide, *X-ray Photoelectron Spectroscopy: An introduction to Principles and Practices*, vol. 2011. 2011.

[84] G. A. Somorjai, *Chemistry in two dimensions: surfaces*. Cornell University Press, 1981.

[85] P. Willmott, *An Introduction to Synchrotron Radiation: Techniques and Applications*. Wiley, 2011.

[86] G. Binnig and H. Rohrer, "Scanning tunneling microscopy," *Surf. Sci.*, vol. 126, no. 1–3, pp. 236–244, 1983.

[87] G. Binnig and C. F. Quate, "Atomic Force Microscope," *Phys. Rev. Lett.*, vol. 56, no. 9, 1986.

[88] G. Haugstad, *Atomic Force Microscopy: Understanding Basic Modes and Advanced Applications*. Wiley, 2012.

[89] W. Liu, H. Li, C. Xu, Y. Khatami, and K. Banerjee, "Synthesis of high-quality monolayer and bilayer graphene on copper using chemical vapor deposition," *Carbon N. Y.*, vol. 49, no. 13, pp. 4122–4130, 2011.

[90] I. Vlassiouk, S. Smirnov, M. Regmi, S. P. Surwade, N. Srivastava, R. Feenstra, G. Eres, C. Parish, N. Lavrik, P. Datskos, S. Dai, and P. Fulvio, "Graphene Nucleation Density on Copper : Fundamental Role of Background Pressure," *J. Phys. Chem. C*, pp. 18919–18926, 2013.

[91] S. Bhaviripudi, X. Jia, M. S. Dresselhaus, and J. Kong, "Role of Kinetic Factors in Chemical Vapor Graphene Using Copper Catalyst," *Nano Lett.*, vol. 10, pp. 4128–4133, 2010.

[92] J. D. Wood, S. W. Schmucker, A. S. Lyons, E. Pop, and J. W. Lyding, "Effect of Polycrystalline Cu Substrate on Graphene Growth by Chemical Vapor Deposition," *Nano Lett.*, vol. 11, pp. 4547–4554, 2011.

[93] Z. Luo, Y. Lu, D. W. Singer, M. E. Berck, L. A. Somers, B. R. Goldsmith, and A. T. C. Johnson, "Effect of Substrate Roughness and Feedstock Concentration on Growth of Wafer-Scale Graphene at Atmospheric Pressure," *Chem. Mater.*, vol. 23, pp. 1441–1447, 2011.

[94] A. Jorio, E. H. M. Ferreira, F. Stavale, C. A. Achete, R. B. Capaz, M. V. O. Moutinho, A. Lombardo, T. S. Kulmala, and A. C. Ferrari, "Quantifying Defects in Graphene via Raman Spectroscopy at Different Excitation Energies," *Nano Lett.*, pp. 3190–3196, 2011.

[95] M. S. Dresselhaus, G. Dresselhaus, and M. Hofmann, "Raman spectroscopy as a probe of graphene and carbon nanotubes," no. November 2007, pp. 231–236, 2008.

[96] C. Wang, Y. Zhou, L. He, T. Ng, and G. Hong, "polydimethylsiloxane by plasma enhanced chemical," pp. 600–605, 2013.

[97] T. Hayashi, B. Wang, A. Berkdemir, Y. A. Kim, R. Cruz-silva, H. R. Gutie, Q. Hao, and A. L. Elı, "Nitrogen-doped graphene: beyond single substitution and enhanced molecular sensing ′," *Sci. Rep.*, vol. 2, pp. 1–8, 2012.

[98] A. Jorio, E. H. M. Ferreira, M. V. O. Moutinho, F. Stavale, C. A. Achete, and R. B. Capaz, "Measuring disorder in graphene with the G and D band," *Phys. Status Solidi b*, vol. 2982, pp. 2980–2982, 2010.

[99] C. Nitrogen-doped and M. G. Sheets, "Large-Scale Growth and Charcterization of Nitrogen-Doped Monolayer Graphene Sheets," *ACS Nano*, vol. 5, no. 5, pp. 4112–4117, 2011.

[100] C. et al. Malitesta, "New findings on polypyrrole chemical structure by XPS coupled to chemical derivatization labelling," *J. Electron Spectros. Relat. Phenomena*, vol. 76, pp. 629–634, 1995.

[101] N. S. Mclntyre and M. G. Cook, "X-Ray Photoelectron Studies on Some Oxides and Hydroxides of Cobalt, Nickel, and Copper," *Anal. Chem.*, vol. 827, no. 11, 1975.

[102] A. Reina, X. Jia, J. Ho, D. Nezich, H. Son, V. Bulovic, M. S. Dresselhaus, and J. Kong, "Large Area , Few-Layer Graphene Films on Arbitrary Substrates by Chemical Vapor Deposition," *Nano Lett.*, vol. 9, no. 1, pp. 30–35, 2009.

[103] H. C. Schniepp, J.-L. Li, M. J. McAllister, H. Sai, M. Herrera-Alonso, D. H. Adamson, R. K. Prud'homme, R. Car, D. A. Saville, and I. A. Aksay, "Functionalized single graphene sheets derived from splitting graphite oxide," *J. Phys. Chem. B*, vol. 110, no. 17, pp. 8535–8539, 2006.

[104] G. D. Yuan, W. J. Zhang, Y. Yang, Y. B. Tang, Y. Q. Li, J. X. Wang, X. M. Meng, Z. B. He, C. M. L. Wu, I. Bello, C. S. Lee, and S. T. Lee, "Graphene sheets via microwave chemical vapor deposition," *Chem. Phys. Lett.*, vol. 467, no. 4–6, pp. 361–364, 2009.